

STRUCTURAL STUDIES ON SUBSTRATE AND INHIBITOR SELECTIVITY OF PHOSPHODIESTERASES

Huanchen Wang

A dissertation submitted to the faculty of the University of North Carolina at Chapel Hill in partial fulfillment of the requirements for the degree of Doctor of Philosophy in the Department of Biochemistry and Biophysics.

Chapel Hill
2006

Approved by

Advisor: Professor Hengming Ke

Reader: Professor Michael Caplow

Reader: Professor Charles W. Carter, Jr.

Reader: Professor Edward J. Collins

Reader: Professor Richard V. Wolfenden

**©2006
Huanchen Wang
ALL RIGHT RESERVED**

ABSTRACT

HUANCHEN WANG: Structural Studies On Substrate And Inhibitor Selectivity Of
Phosphodiesterases
(Under the direction of Dr. Hengming Ke)

Cyclic nucleotide phosphodiesterases (PDEs) control the cellular concentration of “second messengers” adenosine or guanosine 3', 5'-cyclic monophosphate (cAMP or cGMP). All PDEs contain a conserved catalytic domain, but each family possesses different substrate specificity and selective inhibitors. Selective inhibitors of PDEs have been studied as therapeutic agents for various diseases. However, many essential questions about the structure and function of PDEs remain mysteries. This dissertation will focus on inhibitor selectivity and substrate specificity studies of PDEs by X-ray crystallography, mutagenesis and enzymology. The crystal structure of PDE7 and kinetic analysis revealed multiple elements that jointly determinate inhibitor selectivity of PDEs. Crystal structures of PDE5 in complex with inhibitors showed multiple conformations of PDE5, providing insights into the enzyme function and for drug development. Crystal structures of PDE10 and structures of PDE4 subfamilies in complex with a PDE4D selective inhibitor will provide insights into the substrate specificity and subfamily inhibitor selectivity.

To my parents, Rifang Wang and Guange Ma

To my wife, Meiyang Zheng

To my son, Joseph Gen Wang

ACKNOWLEDGEMENTS

I would first like to extend my appreciation to my advisor Dr. Hengming Ke for allowing me conduct my research within his laboratory. His direction and full support directly lead me to succeed in this extraordinary project.

I would like to thank my committee members Dr. Michael Caplow, Dr. Charles W. Carter, Dr. Edward J. Collins and Dr. Richard V. Wolfenden for their advises and direction throughout my years of research.

I thank all the members in Dr. Ke's lab, especially Dr. Qing Huai for her help when I joined Dr. Ke's lab.

I also want to thank my teachers and friends during my time in Chapel Hill. Especially I would like to thank Dr. Jianke Tie, who showed great friendship during my daily life.

Most of all, I would like to thank my parents, Rifang Wang and Guange Ma, my wife, Meiyang Zheng and my son, Joseph Gen Wang; for my sacrifice throughout the years was their sacrifice.

I will not be able to obtain my PhD degree without many people's help and contribution.

TABLE OF CONTENTS

	Page
LIST OF TABLES	viii
LIST OF FIGURES	ix
LIST OF ABBREVIATIONS	xi
CHAPTER I INTRODUCTION OF FUNCTION AND STRUCTURE OF PHOSPHODIESTERASES.....	1
1.1. Regulation of cellular concentration of cAMP and cGMP.....	1
1.2. Superfamily of PDEs.....	2
1.3. PDE inhibitors as therapeutic agents.....	3
1.4. Structural studies on PDEs.....	4
1.5. Focus of this dissertation.....	6
REFERENCES	8
CHAPTER II MULTIPLE ELEMENTS JOINTLY DETERMINE INHIBITOR SELECTIVITY OF CYCLIC NUCLEOTIDE PHOSPHODIESTERASES 4 AND 7.....	20
2.1. Abstract.....	20
2.2. Introduction.....	21
2.3. Experimental procedures.....	22
2.4. Results.....	27

2.5. Discussion.....	33
FOOTNOTES.....	36
REFERENCES.....	37
CHAPTER III MULTIPLE CONFORMATIONS OF PHOSPHODIESTERASE-5: IMPLICATIONS FOR ENZYME FUNCTION AND DRUG DEVELOPMENT.....	53
3.1. Abstract.....	53
3.2. Introduction.....	54
3.3. Experimental procedures.....	56
3.4. Results.....	60
3.5. Discussion.....	69
REFERENCES.....	71
CHAPTER IV CRYSTAL STRUCTURES OF PDE10 IN COMPLEX WITH SUBSTRATES AND PDE4 SUBFAMILIES IN COMPLEX WITH A PDE4D-SELECTIVE INHIBITOR.....	84
4.1. Introduction.....	84
4.2. Crystal structure of PDE10.....	85
4.3. Studies on subfamily selectivity of PDE4 inhibitors.....	89
REFERENCES.....	92
CHAPTER V OTHER WORKS I CONTRIBUTED TO.....	97

LIST OF TABLES

	Page
Table 1.1. Kinetics properties of PDEs.....	19
Table 2.1. Primers for mutations of PDE4 and PDE7.....	48
Table 2.2. Statistics on diffraction data and structure refinement.....	49
Table 2.3. Kinetic parameters of PDE4D2(1-507) and PDE7A1(130-482).....	50
Table 2.4. Interactions of IBMX with PDE7A1.....	51
Table 2.5. Inhibition of PDE4D2 (1-507) and PDE7A1 (130-482) by PDE4 inhibitors.....	52
Table 3.1. Statistics on diffraction data and structure refinement.....	81
Table 3.2. Interactions of sildenafil and icarisid II with PDE5A.....	82
Table 3.3. Kinetic properties of PDE5A1 isolated catalytic domain and its mutants.....	83
Table 4.1. Statistics on diffraction data and structure refinement of PDE10A2(448-789).....	96

LIST OF FIGURES

	Page
Figure 1.1. Signal pathway of cAMP and cGMP.....	11
Figure 1.2. Catalysis by cyclic nucleotide phosphodiesterases.....	12
Figure 1.3. Domain structures of the eleven PDE families.....	13
Figure 1.4. Chemical structures of PDE inhibitors.....	14
Figure 1.5. Structure of the PDE4D2 catalytic domain.....	15
Figure 1.6. Second structure alignment of eight PDE catalytic domains on the basis of three dimensional structures.....	16
Figure 1.7. A putative mechanism for the phosphodiester bond hydrolysis by PDEs.....	17
Figure 1.8. The hydrogen bonding network for binding of the nucleotides at the active site of PDE4 and 5.....	18
Figure 2.1. Chemical structures of PDE inhibitors.....	39
Figure 2.2. The 15% SDS acrylamide gel on the purified proteins.....	40
Figure 2.3. PDE7 kinetic.....	41
Figure 2.4. PDE structures.....	42
Figure 2.5. The inhibitor binding.....	44
Figure 2.6. Inhibition on the cAMP activity of the catalytic domain of the wild type PDE7A1 and its mutants by PDE4 inhibitors.....	46
Figure 2.7. Inhibition on the cAMP activity of the wild type PDE4D2 and its Y329S mutant by PDE4 inhibitors.....	47
Figure 3.1. Chemical structures of PDE5 inhibitors.....	74
Figure 3.2. Structures of PDE5 and its inhibitor complexes.....	75
Figure 3.3. Sildenafil binding.....	77

Figure 3.4. Effects of reducing agent on the activity of PDE5A.....	78
Figure 3.5. Icarisid II binding.....	79
Figure 3.6. Inhibition of the isolated PDE5 catalytic domain of wild type and H-loop deletion mutants by IBMX, icarisid II, and sildenafil.....	80
Figure 4.1. Ribbon diagram of the catalytic domain of PDE10A.....	94
Figure 4.2. Chemical structure of a PDE4D-selective inhibitor NVP-ABE171.....	95

LIST OF ABBREVIATIONS

AC	Adenylyl cyclase
AMP	5' Adenosine monophosphate
cAMP	Adenosine 3',5'- cyclic monophosphate
cGMP	Guanosine 3',5'- cyclic monophosphate
COPD	chronic obstructive pulmonary disease
GAF	<u>c</u> GMP specific PDE, <u>A</u> denylyl cyclase, and <u>F</u> h1A
GC	Guanylyl cyclase
GMP	5' Guanosine monophosphate
IBMX	3-isobutyl-1-methylxanthine
NVP-ABE171	4-(8-benzo[1,2,5]oxadiazol-5-yl-[1,7]naphthyridine-6-yl)-benzoic acid
PAS	<u>P</u> eriod clock protein, <u>A</u> ryl hydrocarbon receptor nuclear translocator, and <u>S</u> ingle-minded protein
PDE	Phosphodiesterase

CHAPTER I

INTRODUCTION OF FUNCTION AND STRUCTURE OF PHOSPHODIESTERASES

1.1. Regulation of cellular concentration of cAMP and cGMP

The second messengers cAMP and cGMP mediate the response of cells to a wide variety of hormones and neurotransmitters and modulate many metabolic processes, including cardiac and smooth muscle contraction, glycogenolysis, platelet aggregation, secretion, lipolysis, ion channel conductance, apoptosis, and growth control (1-7). Signaling of cAMP and cGMP *in vivo* is regulated mainly by three types of enzymes (Figure 1.1): cyclases, phosphodiesterases, and kinases. Intracellular cAMP and cGMP are synthesized by adenylyl cyclase (AC) and guanylyl cyclase (GC) in response to hormones and neurotransmitters (5, 8). The cyclic nucleotides activate cAMP/cGMP-dependent protein kinases (PKA and PKG) that in turn phosphorylate proteins downstream in the signaling pathways (9-11). Cyclic nucleotide phosphodiesterase (PDE) terminate the cAMP and cGMP signals by hydrolyzing the second messengers to 5'-AMP and 5'-GMP (Figure 1.2).

1.2. Superfamily of PDEs

PDEs comprise a large superfamily of enzymes. The 21 genes in human genome can be categorized into 11 families for their distinctive catalytic and regulatory properties, primary sequences, and sensitivities to PDE inhibitors. Alternative mRNA splicing of the 21 genes

generates over 60 isoforms of PDE in various human tissues (12-21). The PDE molecules can be divided into three regions: an N-terminal splicing region, a regulatory domain, and a catalytic domain near the C-terminus (Figure 1.3). The function of the N-terminal splicing region of the PDE families is unknown. The regulatory domains of PDEs contain various structural motifs and are assumed to play roles in the regulation of the catalytic activities of PDEs or in cross talk with other signaling pathways (21-23). Close at the C-terminus, a catalytic domain of about 300 amino acids conserve in all PDEs, but no homology is found in other regions. The catalytic domains share 65% or greater amino acid sequence identity in the same PDE family, whereas the amino acid identity drops to 40% or lower across families.

Each PDE family has its individual substrate preference for cAMP and cGMP. Of the 11 families of PDEs thus far identified, the PDE families 4, 7, and 8 prefer to hydrolyze cAMP while PDE5, 6 and 9 are cGMP specific. PDE1, 2, 3, 10 and 11 enzymes show activities toward both cAMP and cGMP (21) (Table 1.1). Thus, it has been a mystery how the similar active sites of PDEs distinguish the subtle differences between cAMP and cGMP (Figure 1.2).

1.3. PDE inhibitors as therapeutic agents

The conservation of the catalytic domains would predict that members in the PDE families have common inhibitors. Indeed, several non-selective inhibitors of PDEs have been identified. For example, theophylline (Figure 1.4), a classical drug for treatment of asthma, is a non-selective PDE inhibitor (24, 25). On the other hand, each family of PDE possesses selective inhibitors that bind competitively to the conserved active site. For example,

roflumilast (Figure 1.4) is a PDE4 selective inhibitor with IC_{50} of 0.8 nM for PDE4 and IC_{50} of 4 μ M for PDE5 (26). Sildenafil (ViagraTM, Figure 1.4) is a PDE5 selective inhibitor with IC_{50} of 3.5 nM for PDE5 and IC_{50} of 8 μ M for PDE4 (17). It remains unclear how PDEs present selectivity on different inhibitors.

In the past several decades, selective inhibitors of PDEs have been widely studied as therapeutics of cardiotoxic agents, vasodilators, smooth muscle relaxants, antidepressants, antithrombotic compounds, antiasthma, and agents for improving cognitive functions such as learning and memory (27-36). Many PDE inhibitors have been tested in clinical trials or have already entered the marketplace. For example, vinpocetine, a PDE1 inhibitor, was tested for enhancing cognitive function and cerebrovascular health memory. The PDE3 selective inhibitor cilostazole (PletalTM, Figure 1.4) has been approved as a drug for reduction of symptoms of intermittent claudication. The PDE5 inhibitors sildenafil (ViagraTM, Figure 1.4), vardenafil (LevitraTM), and tadalafil (CialisTM) are drugs for treatment of male erectile dysfunction. Selective inhibitors of PDE4 form the largest group among any PDE families and have been studied as anti-inflammatory drugs for treatment of asthma and chronic obstructive pulmonary disease (COPD) and also as therapeutic agents against rheumatoid arthritis, multiple sclerosis, type II diabetes, septic shock, atopic dermatitis and other autoimmune diseases (32,37-42). Over 450 patents on PDE4 inhibitors have been published (40), but no PDE4 selective inhibitor has been approved for treatment of diseases. PDE4 inhibitors cilomilast and roflumilast (Figure 1.4) have shown their great potency for treatment of asthma and COPD (32, 39-42), but the side effects such as emesis at high dosage limit their practical application.

The side effects of the PDE inhibitors are generally thought to be the consequences of non-selective inhibition on other families or sub-families of PDEs. For example, the side effect headache of sildenafil presumably results from the non-selective binding of sildenafil to PDE4D or PDE1 in brain (17) and vision disturbance after administration of sildenafil may be due to the non-selective inhibition of sildenafil on PDE6 (43). Thus, improvement of the inhibitor selectivity is an essential step to enhance efficacy and to reduce side effects of the drugs. This is especially critical because over 60 isoforms of PDEs exist in human body.

1.4. Structural studies on PDEs

Since publication of the first crystal structure of the catalytic domain of PDE4B in 2000, structures of the catalytic domains of seven PDE families have been published: PDE1B (44), PDE2A (45), PDE3B (46), PDE4B and PDE4D (44, 47-54), PDE5A (44,52,55), PDE7A (56), and PDE9A (57), and a new crystal structure of PDE10A will be reported in this dissertation. In addition, the structures of a regulatory domain of PDE2A (58) and a fragment of PDE4D5 splicing region (59) have been reported. The catalytic domains of most PDE families contain sixteen α -helices, fourteen of which are superimposable and thus define a conserved core (about 300 amino acids) of the catalytic domains for PDE families (Figures 5 & 6).

The structural studies have leded a preliminary understanding on the hydrolysis mechanism, substrate specificity, and inhibitor selectivity. A mechanism by which PDE hydrolyzes cyclic nucleotides was proposed (51, Figure 7). In this model, the interactions of

cAMP phosphate with two metal ions polarize the phosphodiester bond so as to make the phosphorus atom partially positively charged. A water or hydroxide ion that bridges two metals is activated by Asp318 and attacks the phosphorus. His160 then serves as a proton donor for completion of the phosphodiester bond hydrolysis. This mechanism may be universal for all class I PDEs since the metal binding residues are highly conserved across all the PDE families.

Structural studies have identified a conserved glutamine that plays a critical role in binding of substrates and inhibitor (46; 50-52). A “glutamine switch” mechanism has been proposed for differentiation of substrate specificity (44) on basis of the observation of that side chain of the invariant glutamine shows an opposite orientation in the crystals of PDE4 and PDE5. In the structure of the PDE4D2-AMP complex, the orientation of the side chain (Residue Gln369) is fixed by a hydrogen bond with Tyr329 (Figure 1.8). In contrast, the orientation of the side chain (residue Gln817) is rotated about 180° and is fixed by Gln775 in the structure of the PDE5A1-GMP complex. The “glutamine switch” mechanism assumes a free rotation of the invariant glutamine in the PDE families that have dual specificity. However, the recently structure of PDE2A showed that Gln859 already forms a hydrogen bond with Tyr827 (45). Thus, the mechanism of “glutamine switch” need further studies.

A large number of the crystal structures of PDE in complex with both non-selective and selective inhibitor identified a common binding pattern for all PDE inhibitors: stacking against a conserved phenylalanine and forming a hydrogen bond network with a conserved glutamine. These two factors probably form a core of a common subpocket for binding of all

inhibitors. However, it remains unknown what are determinants for selective binding of structural distinct inhibitors in different PDE families and if each PDE family has its characteristic combination of recognition elements or shares certain elements with other PDE families.

1.5. Focus of this dissertation

Working in Dr. Ke's lab, I have focused on the issues of substrate specificity and inhibitor selectivity of PDEs by X-ray crystallography and enzymatic approaches. In this dissertation, I will report crystal structures of PDE7 and the kinetic analysis on the mutants of PDE4 and PDE7, to address the issue of inhibitor selectivity in these PDE families in chapter II. In chapter III, I will describe the crystal structures of PDE5 in the unliganded form and in complex with inhibitors sildenafil and icarid II and discuss multiple conformations of PDE5 and the implication on the enzyme function and drug development. In chapter IV I will report the recently progress on expression, purification, and structural determination of PDE PDE4A, PDE4B, PDE4C, PDE4D, and PDE10A. Finally, I will list and attach the reprints of other works that I contributed to during my PhD studies, including the crystal structures of PDE4D in complex with enantiomer inhibitors, rolipram, PDE9 in complex with IBMX, DJ-1, *E. Coli* Hsp90. and a complex involving a mouse TCR and a human MHC molecule.

REFERENCES

1. Houslay, M. D. (1998) *Cell & Develop. Biol.*, **9**, 161-167.
2. Pelligrino D.A. , Wang Q. (1998) *Prog Neurobiol.* **56**, 1-18.
3. Antoni, F. (2000) *Front. Neuroendocrin.*, **21**, 103-132.
4. Carvajal J.A., Germain A.M., Huidobro-Toro J.P., Weiner C.P.. (2000) *Cell Physiol.* **184**, 409-420.
5. Lucas K.A., Pitari G.M., Kazerounian S., Ruiz-Stewart I., Park J., Schulz S., Chepenik K.P., Waldman S.A. (2000) *Cell. Signalling.* **14**, 493-498.
7. Chin K.V., Yang W.L., Ravatn R., Kita T., Reitman E., Vettori D., Cvijic M.E., Shin M., Iacono L. (2002) *Ann N Y Acad Sci.* **968**, 49-64.
8. Taussig, R. & Gilman, A. G. (1995) *J. Biol. Chem.*, **270**, 1-4.
9. Houslay, M. D. & Milligan, G. (1997) *TIBS*, **22**, 217-224.
10. Francis S.H., Corbin J.D.. (1999) *Crit Rev Clin Lab Sci.* **36**, 275-328.
11. Lincoln T.M., Dey N., Sellak H. (2001) *J Appl Physiol.* **91**, 1421-1430.
12. Beavo, J. A. (1995) *Physiol. Rev.*, **75**, 725-748.
13. Thompson, W. J. (1991) *Pharmac. Ther.*, **51**, 13-33.
14. Manganiello, V. C., Murata, T., Taira, M., Belfrage, P. & Degerman, F. (1995a) *Arch. Biochem. Biophys.*, **322**, 1-13.
15. Müller, T., Engels, P., & Fozard, J. R. (1996) *TIPS*, **17**, 294-298.
16. Torphy, T. J. (1998) *Am. J. Respir. Crit. Care Med.*, **157**, 351-370.
17. Corbin, J. D. & Francis, S. H. (2002) *Int. J. Clin. Pract.* **56**, 453-459.
18. Dousa, T. P. (1999) *Kidney Internat.* **55**, 29-62.
19. Juilfs, D. M., Soderling, S., Burns, F., & Beavo, J. A. (1999) *Rev. Physiol. Biochem. Pharmacol.*, **135**, 67-104.
20. Soderling S.H. & Beavo J.A. (2000) *Curr Opin Cell Biol.* 12(2):174-9.

21. Mehats C., Andersen C.B., Filopanti M., Jin SL., Conti M. (2002) *Trends in Endocrinol. & Metabolism*. **13**, 29-35.
22. Manganiello, V. C., Taira, M., Degerman, F. & Belfrage, P. (1995b) *Cell Signal.*, **7**, 445-455.
23. Degerman, E., Belfragem P., & Manganiello, V. C. (1996) *Biochem. Soc. Trans.* **24**, 1010-1013.
24. Weishaar R.E., Burrows S.D., Kobylarz D.C., Quade M.M., Evans D.B. (1986) *Biochem Pharmacol.* **35**, 787-800.
25. Spina D. (2003) *Curr Opin Pulm Med.* **9**, 57-64.
26. Hatzelmann, A. and Schudt, C. (2001) *J. Pharmacol. Exp. Ther.* **297**, 267-279.
27. Torphy, T. J. and Udem, B. J. (1991) *Thorax*, **46**, 512-524.
28. Torphy T. J. Livi, G. P., and Christensen, S. B. (1993) *DN&P*, **6**, 203-214.
29. Movsesian M.A. (2000) *Expert Opin. Investigational Drugs.* **9**, 963-73.
30. Truss, M. C., Stief, C. G., Uckert, S., Becker, A. J., Wafer, J., Schultheiss, D., and Jonas, U. (2001) *World J. Urol.* **19**, 344-350.
31. Liu, Y., Shakur, Y., Yoshitake, M., and Kambayashi, J. J. (2001) *Cardiovascular Drug Rev.* **19**, 369-86.
32. Huang, Z., Ducharme, Y., MacDonald, D., and Robinchaud, A. (2001) *Curr. Opin. Chem. Biol.*, **5**, 432-438.
32. Rotella, D. P. (2002) *Nature Rev. Drug Discovery* **1**, 674 – 682.
34. Schrör K. (2002) *Diabetes Obes Metab.* **4** Suppl 2, S14-9.
35. Abdel-Hamid IA. (2004) *Drugs* **64**, 13-26.
36. Crowe S.M. & Streetman D.S.(2004) *Ann Pharmacother.* **38**, 77-85.
37. Barnette, M.S. (1999) *Fortschritte der Arzneimittelforschung - Progress in Drug Research*, **53**, 193-229.
38. Piazz, V. D. & Giovannoni, P. (2000) *Eur. J. Med. Chem.*, **35**, 463-480.
39. Barnette, M. S., Underwood, D. C. (2000) *Curr. Opin. Pulmonary Med.*, **6**, 164-169.

40. Souness, J. E., Aldous, D., & Sargent C. (2000) *Immunopharmacology*, **47**, 127-162.
41. Giembycz, M. A. (2002) *Monaldi Arch. Chest Dis.* **57**, 48-64.
42. Sturton, G. & Fitzgerald, M. (2002) *Chest*, **121**, 192s-196s.
43. Pomeranz, H. D. and Bhavsar, A. R. (2005) *J Neuroophthalmol.* **25**, 9-13.
44. Zhang K.Y., Card G.L., Suzuki Y., Artis D.R., Fong D., Gillette S., Hsieh D., Neiman J., West B.L., Zhang C., Milburn M.V., Kim S.H., Schlessinger J., Bollag G. (2004) *Mol Cell.* **15**, 279-286.
45. Iffland A., Kohls D., Low S., Luan J., Zhang Y., Kothe M., Cao Q., Kamath A.V., Ding Y.H., Ellenberger T. (2005) *Biochemistry* **44**, 8312-8325.
46. Scaping G., Patel S.B., Chung C., Varnerin J.P., Edmondson S.D., Mastracchio A., Parmee E.R., Singh S.B., Becker J.W., Van der Ploeg L.H., Tota M.R. (2004) *Biochemistry* **43**, 6091-6100.
47. Xu, R.X., Hassell, A.M., Vanderwall, D., Lambert, M.H., Holmes, W.D., Luther, M.A., Rocque, W.J., Milburn, M.V., Zhao, Y., Ke, H., and Nolte, R.T. (2000). *Science* **288**, 1822-1825.
48. Xu R.X., Rocque W.J., Lambert M.H., Vanderwall D.E., Luther M.A., Nolte R.T. (2004) *J. Mol. Biol.* **337**, 355-365.
49. Lee, M.E., Markowitz, J., Lee, J.O., and Lee, H. (2002). *FEBS Lett*, **530**, 53-58.
50. Huai, Q., Wang H., Sun, Y., Kim, H.Y., Liu, Y., and Ke, H. (2003a) *Structure*, **11**, 865-873.
51. Huai, Q., Colicelli, J., and Ke, H. (2003b) *Biochemistry* **42**, 13220-13226.
52. Huai, Q., Liu, Y., Francis, S. H., Corbin, J. D., and Ke, H. (2004a) *J. Biol. Chem.* **279**, 13095-13101.
53. Card G.L., England B.P., Suzuki Y., Fong D., Powell B., Lee B., Luu C., Tabrizizad M., Gillette S., Ibrahim P.N., Artis D.R., Bollag G., Milburn M.V., Kim S.H., Schlessinger J., Zhang KY. (2004) *Structure* **12**, 2233-2247.
54. Card G.L., Blasdel L., England B.P., Zhang C., Suzuki Y., Gillette S., Fong D., Ibrahim P.N., Artis D.R., Bollag G., Milburn M.V., Kim S.H., Schlessinger J., Zhang K.Y. (2005) *Nat Biotechnol.* **23**, 201-207.

55. Sung, B. J., Hwang, K. Y., Jeon Y. H., Lee, J. I., Heo, Y. S., Kim, J. H., Moon, J., Yoon, J. M., Hyun, Y. L., Kim, E., Eum, S. J., Park, S. Y., Lee, J. O., Lee, T. G., Ro, S., and Cho, J. M. (2003) *Nature* **425**, 98-102.
56. Huai, Q., Wang, H., Zhang, W., Colman, R.W., Robinson, H., and Ke, H. (2004b) *Proc. Natl. Acad. Sci. USA*, **101**, 9624-9629.
57. Wang, H., Liu, Y., Chen, Y., Robinson, H., and Ke, H. (2005) *J. Biol. Chem.* 2005 Sep 2;280(35):30949-30955.
58. Martinez S.E., Wu A.Y., Glavas N.A., Tang X.B., Turley S., Hol W.G., Beavo J.A. (2002) *Proc. Natl. Acad. Sci., USA*. **99**, 13260-13265.
59. Smith, K. J., Scotland, G., Beattie, J., Trayer, I. P., Houslay, M. D. (1996) *J. Biol. Chem.* **271** pp. 16703-16711

Figure 1.1. Signal pathway of cAMP and cGMP. The second messengers cAMP and cGMP are synthesized by adenyl or guanylyl cyclases and hydrolyzed by phosphodiesterases, and activate protein kinases for regulation of biological processes.

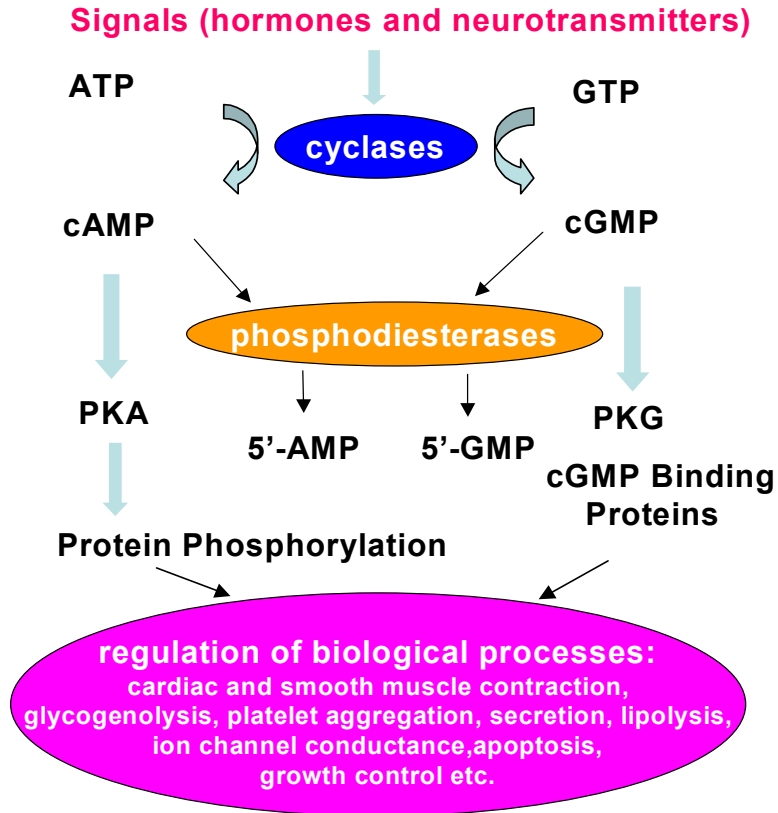


Figure 1.2. Catalysis by cyclic nucleotide phosphodiesterases.

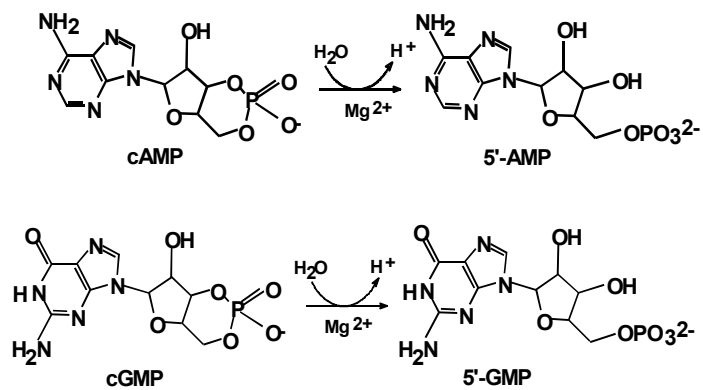
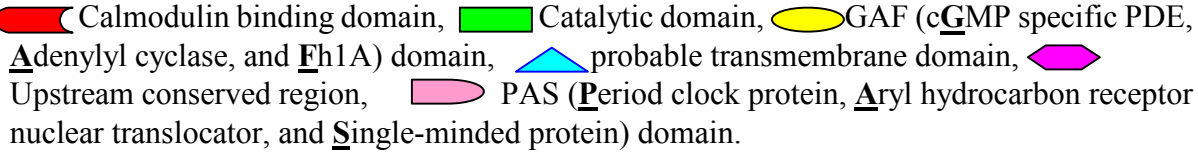


Figure 1.3. Domain structures of the eleven PDE families. PDE nomenclature has been made as the following example: PDE4D2 is defined as family 4, D gene or subfamily D, isoform 2).


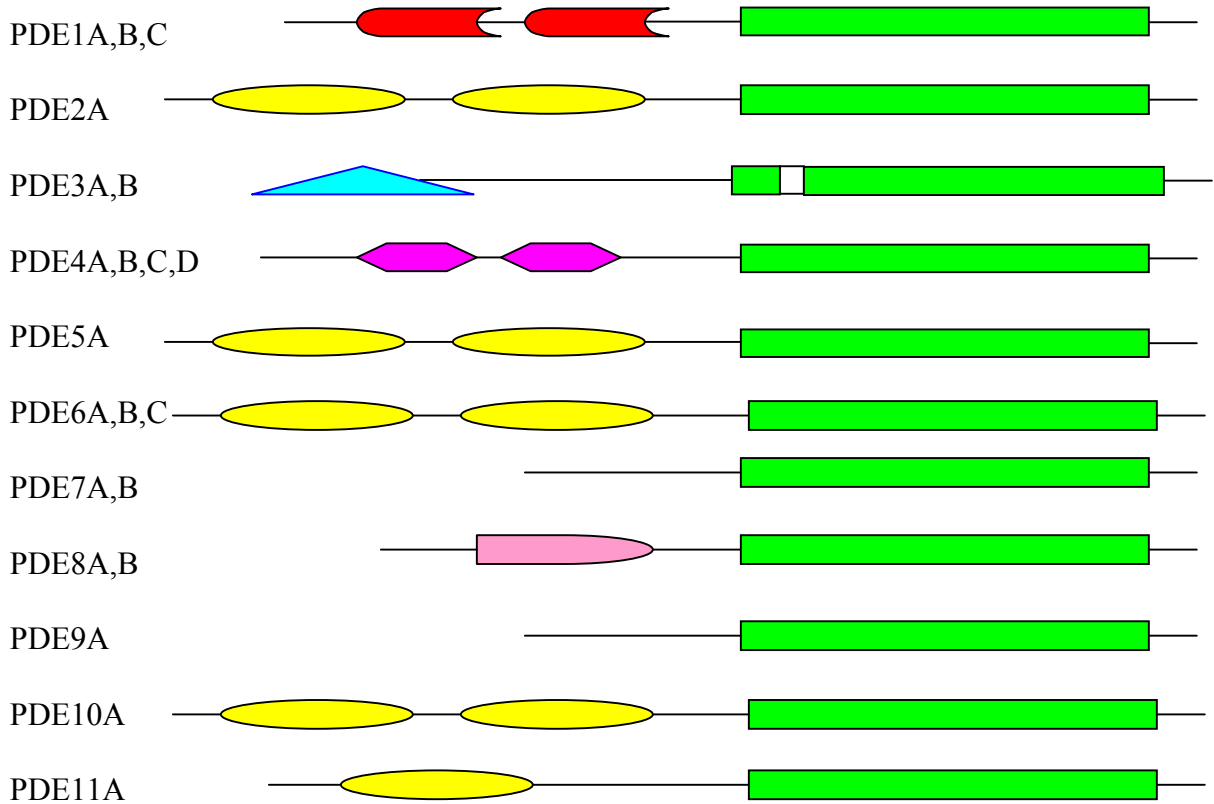


Figure 1.4. Chemical structures of PDE inhibitors. Vinpocetine is a PDE1 selective inhibitor. Cilostazol is a PDE3 selective inhibitor. Rolipram, roflumilast, cilomilast are PDE4-selective inhibitors. Sildenafil, tadalafil, vardenafil are PDE5-selective inhibitors. Theophylline and IBMX are non-selective inhibitors for all PDEs.

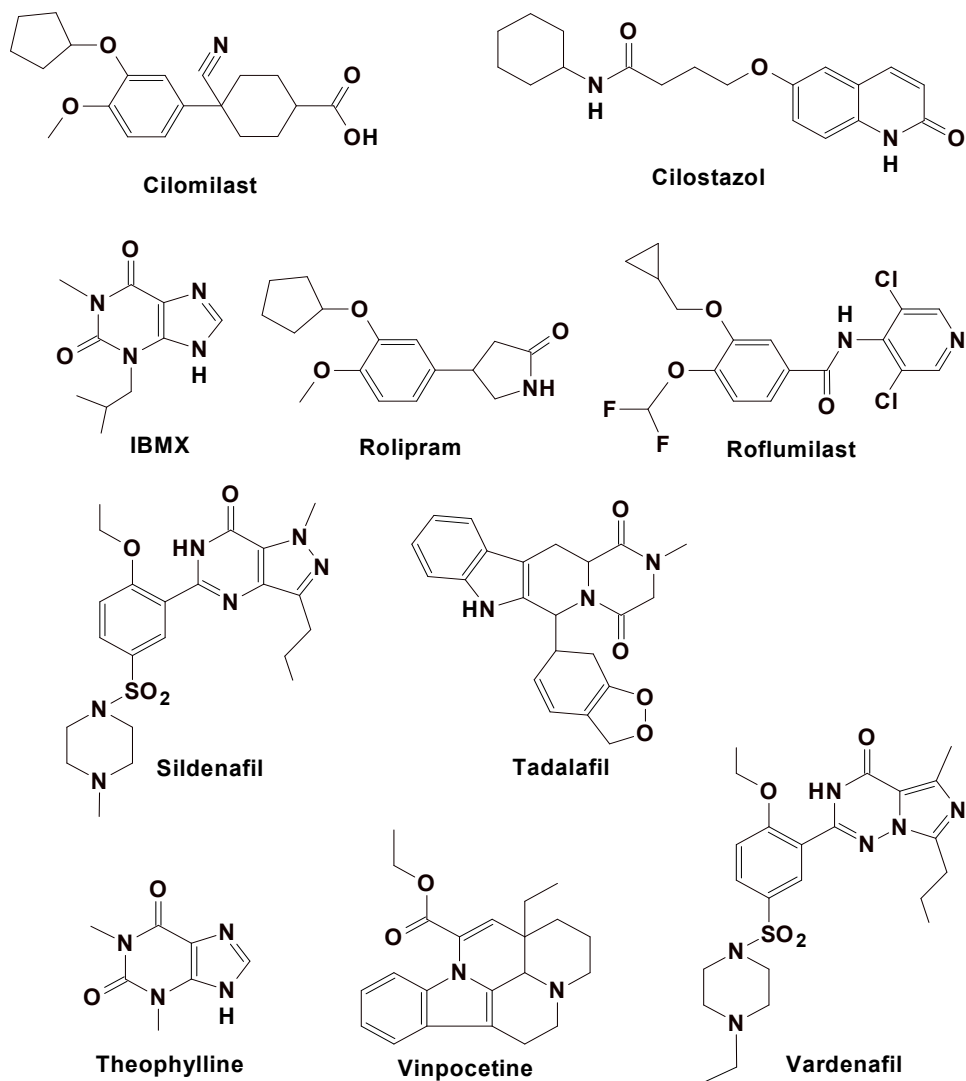
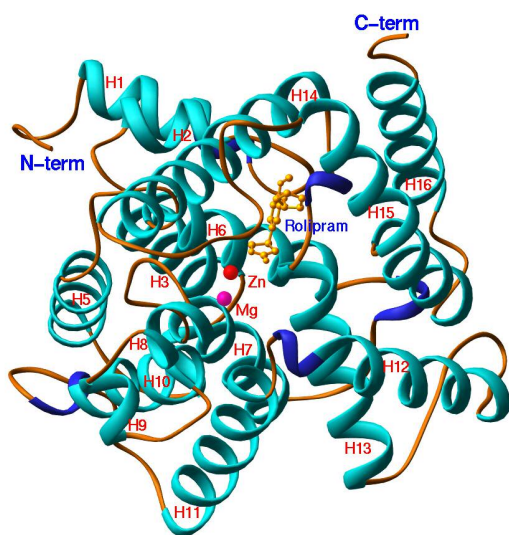
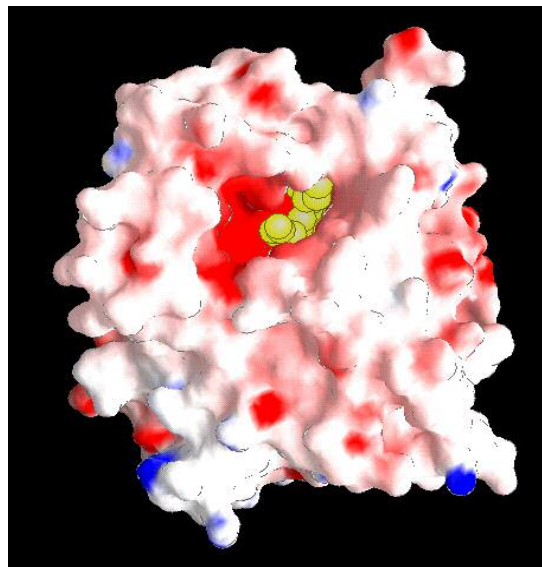


Figure 1.5. Structure of the PDE4D2 catalytic domain. (A) Ribbon diagram. Alpha-helices are shown in cyan and 3_{10} helices are in blue. Rolipram is represented by the golden ball-sticks. (B) Surface presentation of PDE4D2 catalytic domain. Red color represents negatively charged oxygen and blue is for nitrogen. The golden balls are atoms of rolipram.



(A)



(B)

Figure 1.6. Second structure alignment of eight PDE catalytic domains on the basis of three dimensional structures. The unliganded PDE5 is used in the alignment.

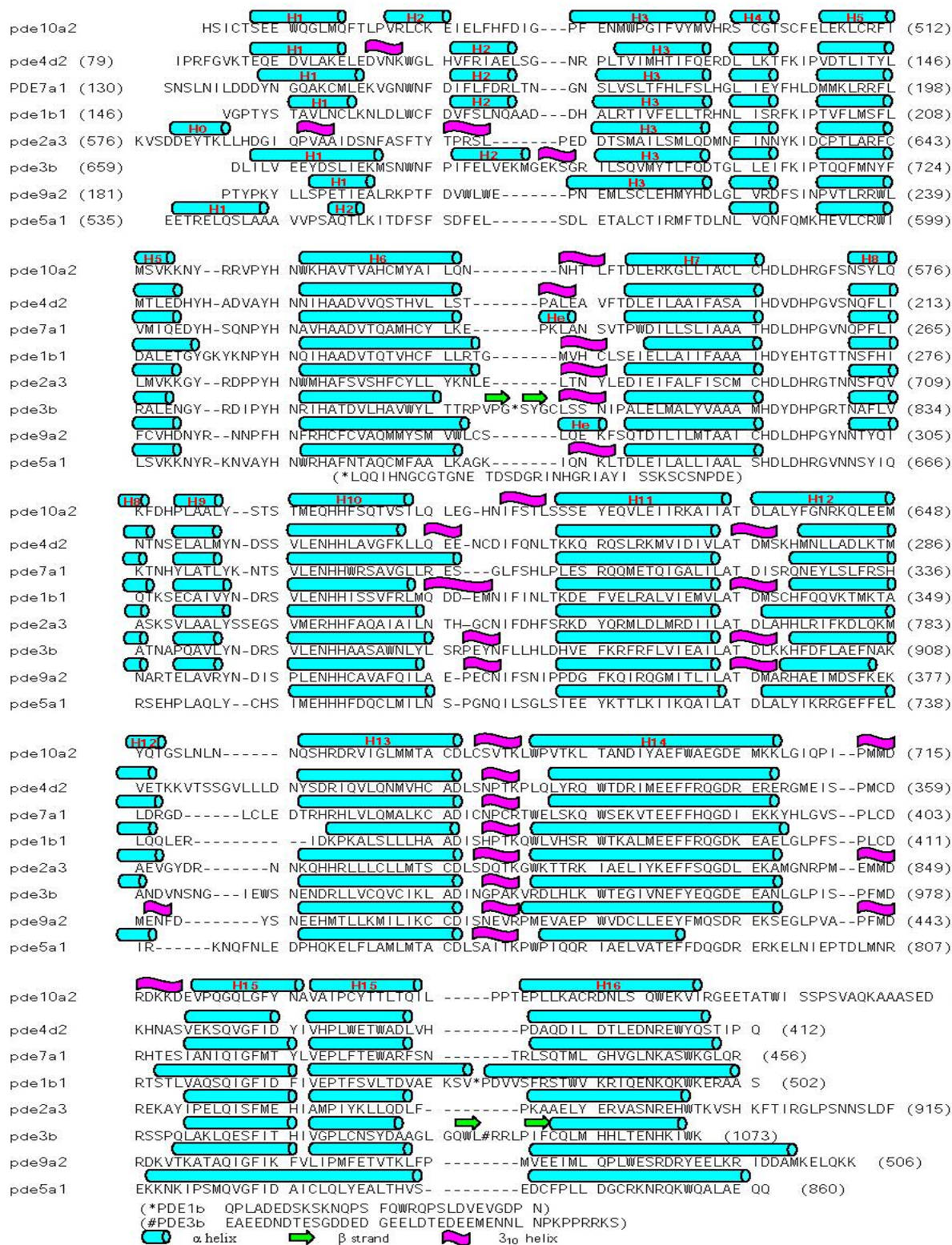


Figure 1.7. A putative mechanism for the phosphodiester bond hydrolysis by PDEs (51).

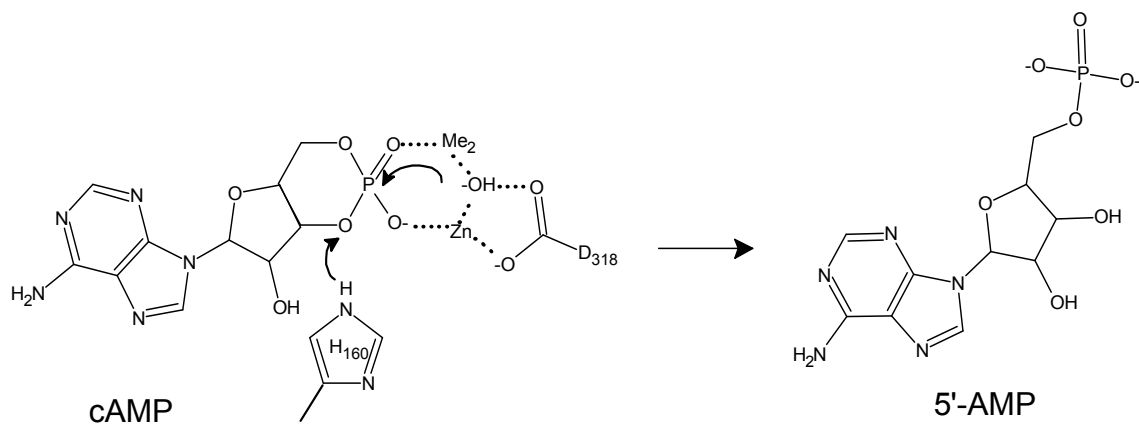
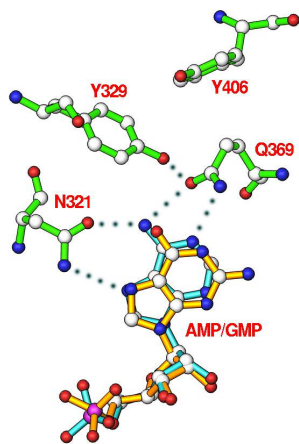
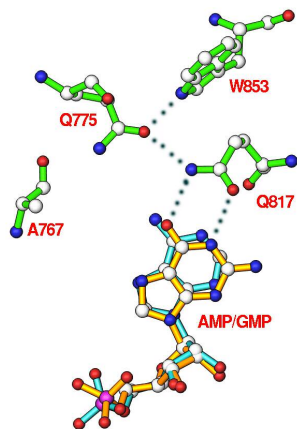


Figure 1.8. The hydrogen bonding network for binding of the nucleotides at the active site of PDE4 and 5. The AMP (cyan bonds) and GMP (golden bonds) were modeled on basis of the superposition of the crystal structures over PDE4D-AMP or PDE5A-GMP.



(PDE4D2)



(PDE5A1)

Table 1.1. Kinetics properties of PDEs (20).

	cAMP (K_M μ M)	cGMP (K_M μ M)
PDE1	1-30	3
PDE2	30-100	10-30
PDE3	0.1-0.5	0.1-0.5
PDE4	0.5-4	>50
PDE5	>40	1.5
PDE6	2000	60
PDE7	0.2	>1000
PDE8	0.7	>100
PDE9	>100	0.07
PDE10	0.05	3
PDE11	1	0.5

CHAPTER II

MULTIPLE ELEMENTS JOINTLY DETERMINE INHIBITOR SELECTIVITY OF CYCLIC NUCLEOTIDE PHOSPHODIESTERASES 4 AND 7

2.1. Abstract

Phosphodiesterase (PDE) inhibitors have been widely studied as therapeutics for treatment of human diseases. However, the mechanism by which each PDE family recognizes selectively a category of inhibitors remains a puzzle. In this chapter I will report the crystal structure of PDE7A1 catalytic domain in complex with non-selective inhibitor 3-isobutyl-1-methylxanthine and kinetic analysis on the mutants of PDE7A1 and PDE4D2. The structural study suggests at least three elements play critical roles in inhibitor selectivity: 1) the conformation and position of an invariant glutamine, 2) the natures of scaffolding residues, and 3) residues that alter shape and size of the binding pocket. Kinetic analysis shows that the single PDE7 to PDE4 mutations increase the sensitivity of PDE7 to PDE4 inhibitors by a few fold, but are not sufficient to render the engineered enzymes comparable with the wild types. The triple S373Y/S377T/I412S mutation of PDE7A1 produces a PDE4-like enzyme, implying that multiple elements must work together to determine inhibitor selectivity.

2.2. Introduction

Phosphodiesterase family 7 (PDE7) consists of two genes, PDE7A and PDE7B. Alternative RNA splicing of PDE7 genes generates PDE7A1 (482 amino acids), PDE7A2 (456 aa), PDE7A3 (425 aa), PDE7B1 (450 aa), and PDE7B2 (583 aa). PDE7 is abundantly expressed in immune cells and has been implicated in T lymphocyte activation (1-5), although there is a report that PDE7A knockout mice showed no deficiency in T cell proliferation (6). Like PDE4, PDE7 prefers to hydrolyze cAMP with a K_M value of 0.03 to 0.2 μM (7-11). However, PDE7 is not sensitive to PDE4 inhibitors such as rolipram (Figure 2.1), and thus was originally named as “rolipram-insensitive PDE family”. To understand the inhibitor selectivity of the PDE7 and PDE4 families, I have determined the crystal structure of the PDE7A1 catalytic domain in complex with 3-isobuty-1-methylxanthine (IBMX) and performed mutagenesis on PDE7A1 and PDE4D2. These studies show that several key residues must work together to switch the inhibitor selectivity between PDE4 and PDE7, and thus provide a valuable insight into selectivity of PDE inhibitors. The results have been published in Journal of Biological Chemistry (12).

2.3. Experimental procedures

Subcloning, protein expression and purification-- The cDNA of PDE7A1 was purchased from American Type Culture Collection (ATCC, BE782968) and subcloned into the vector pET32a- Δ following the standard protocols. The S-tag and enterokinase site in the commercial pET32a were deleted to generate the modified vector pET32a- Δ . A pair of oligonucleotide primers of GCCTGGATCCTCAAATTCCTAAAC and CGCGCTCGAGTTATGATAACCGATTTTC was synthesized for amplification of the PDE7A1 coding region of amino acids 130-482 by PCR. The amplified PDE7A1 DNA and the expression vector pET32a- Δ were separately digested by the restriction enzymes BamHI and XhoI, purified from agarose gel, and then ligated by T4 DNA ligase. The plasmid pET32- PDE7A1 (130-482) was transferred into *E. coli* strain BL21 (codonplus) for overexpression. The *E. coli* cell carrying pET-PDE7A1 was grown in 2xYT medium at 37°C to absorption A600 = 1.0 and then 0.1 mM isopropyl β -D-thiogalactopyranoside was added for further growth at 15°C for 12-16 hours. The cells were harvested and frozen at -80 °C for use.

The catalytic domain of PDE7A1 was purified with three chromatographic columns of Ni-NTA (Qiagen), Q-sepharose (Amersham Biosciences), and Sephacryl S300 (Amersham Biosciences). The Ni-NTA affinity column was washed with a buffer of 20 mM Tris.base, pH 8.0, 300 mM NaCl, 15 mM imidazole and 1 mM β -mercaptoethanol, and PDE7A1 was eluted out with a buffer of 20 mM Tris.base, pH 8.0, 50 mM NaCl, 150 mM imidazole, and 1 mM β -mercaptoethanol. After removal of the His-tag by thrombin cleavage, the PDE7A1 catalytic domain was loaded into Q-sepharose column, washed with 20 mM Tris.base, pH 7.5, 100 mM NaCl, 1 mM β -ME, 1 mM MgCl₂, and 10% glycerol, and eluted out with a similar buffer

but 200 mM NaCl. The PDE7A1 was finally purified by passing through Sephacryl S300 column in a buffer of 20 mM Tris.base, pH 7.5, 50 mM NaCl, 1 mM β -mercaptoethanol, and 1 mM MgCl₂. A typical batch of purification yielded about 5 mg PDE7A1 from 4 liters of cell culture. The purified protein showed a single band in SDS PAGE and native PAGE and is estimated to have purity of better than 95% (Figure 2.2). The purified catalytic domain of PDE7A1 was concentrated to 5 mg/ml and stored at -80 °C for use.

The cDNA clone of full-length PDE4D2 was purchased from American Type Culture Collection (BF697394) and subcloned into pET15b. The plasmid pET- PDE4D2 (1-507) was transferred into *E. coli* strain BL21 (codonplus) for overexpression. The *E. coli* cell carrying pET-PDE4D2 was grown in LB medium at 37°C to absorption A₆₀₀ = 0.7 and then 0.1 mM isopropyl β -D-thiogalactopyranoside was added for further growth at 15°C for 20 hours. The cells were harvested and frozen at -80 °C. The full-length PDE4D2 (1-507) was purified with three chromatographic columns of Ni-NTA (Qiagen), Q-sepharose (Amersham Biosciences), and Sephacryl S300 (Amersham Biosciences). The Ni-NTA affinity column was washed with a buffer of 20 mM Tris.base, pH 8.0, 300 mM NaCl, 15 mM imidazole and 1 mM β -mercaptoethanol, and eluted with similar buffer but 50 mM NaCl and 150 mM imidazole. After removal of the His-tag by thrombin digestion, the full-length PDE4D2 was loaded into Q-sepharose column, washed with 20 mM Tris.base, pH 7.5, 200 mM NaCl, 1 mM β -ME, 1 mM EDTA, and 10% glycerol, and eluted out with a similar buffer but 300 mM NaCl. The PDE4D2 was finally purified by passing through Sephacryl S300 column in a buffer of 20 mM Tris.base, pH 7.5, 50 mM NaCl, 1 mM β -mercaptoethanol, and 1 mM EDTA. A typical batch of purification yielded about 20 mg PDE4D2 from 2 liters of cell culture. The purified

protein showed a single band in SDS PAGE and native PAGE and is estimated to have purity of better than 95% (Figure 2.2).

The mutants of PDE4D2-(1-507) and PDE7A1-(130-482) were produced with a QuikChangeTM site-directed mutagenesis kit and verified by DNA sequencing. The primers for PCR of the mutation are listed in Table 2.1.

All mutants were overexpressed in BL21 (codonplus) and purified using the same procedure as that for the wild types. The expression levels of the PDE7A1 mutants are comparable with that of the wild type PDE7A1. The purified PDE7A1 mutants are estimated to have purity >95% as shown by the SDS gel (Figure 2.2).

Crystallization and structure determination -- Crystals of PDE7A1-IBMX were grown by vapor diffusion. The catalytic domain of 5 mg/mL PDE7A1 (amino acids 130-482) in a storage buffer of 50 mM NaCl, 20 mM Tris-HCl (pH 7.5), 1 mM β -mercaptoethanol, and 1 mM EDTA was mixed with 1 mM IBMX, and crystallized by hanging drop at 4°C. The protein drops contained 2 μ l PDE7A1-IBMX and 2 μ l well buffer of buffer 0.6 - 0.8 M $(\text{NH}_4)_2\text{SO}_4$, 2.5 - 5 mM β -mercaptoethanol, 10 mM EDTA, 0.1 M Tris-HCl, pH 7.5. The well buffer plus 20% glycerol was used as the cryo-solvent for freezing the crystals in liquid nitrogen. Diffraction data were collected on beamline X29 of National Synchrotron Light Source. The PDE7A1-IBMX crystal has the space group $P3_121$ with cell dimensions of $a = 115.8$, and $c = 64.3$ Å. The diffraction images were automatically indexed and integrated by the subroutine Denzo of HKL, and then all the images were scaled and reduced by subroutine

Scalepack of HKL(13). The statistics on the data process are shown in Table 2.2. The structure of PDE7A1-IBMX was solved by molecular replacement program AMoRe (14), using the catalytic domain of PDE4D2 as the initial model (15). The structure determination by AMoRe includes two steps: rotation function and translation search. The rotation function of AMoRe produced a peak with correlation coefficient of 0.12 for 3795 reflections at 4-8 Å resolution, which is about 6 times the remaining solutions. A further search of the peak by the translation function of AMoRe yielded a correlation coefficient of 0.73 and R-factor of 0.31 for 3795 reflections at 4-8 Å resolution. The phases from the molecular replacement were improved by the density modification package of program CCP4 (16). The atomic model output from AMoRe was displayed in a Silicon graphic system and amino acid differences between PDE4 and PDE7 and residue positions were built by program O (17) for the best fit to the electron density maps. The structure was refined by program CNS (Cystallography and NMR System, 18).

Assay of phosphodiesterase activities--The enzymatic activities of the catalytic domains of PDE7A1-(130-482) and full-length PDE4D2-(1-507) and their mutants were assayed by incubating the enzymes with 100 µl reaction mixture of 50 mM Tris·HCl (pH 8.5), 50 mM MgCl₂, 5 mM dithiothreitol,, and ³H-cAMP or ³H-cGMP (30,000 cpm per assay, Sigma-Aldrich) at room temperature for 10 min. The reactions were terminated by addition of 200 µl 0.2 M ZnSO₄ when 20%-35% of cAMP or cGMP was hydrolyzed. The reaction product ³H-AMP or ³H-GMP was precipitated by addition of 200 µl 0.25 M Ba(OH)₂ (Sigma-Aldrich), while unreacted ³H-cAMP or ³H-cGMP remained in the supernatant. Radioactivity of the supernatant was measured in 3.5 ml liquid scintillation cocktails

(ScintiSafe PlusTM 50%, Fisher Scientific) by a LKB RackBeta 1214 counter. The activity was measured at nine concentrations of cAMP or cGMP and each measurement was repeated three times. V_{\max} and K_M values were calculated by the linear plots of Lineweaver–Burk and Eadie-Hofstee (Figure 2.3). Protein concentrations were calculated from the extinction coefficients at O.D. 280 nm, which were calculated by program ProtoParam (ExpASy). For measurement of inhibition, 10-12 concentrations of inhibitors were used under the substrate concentration of one tenth of K_M and the enzyme concentration range of 10-300 ng/ml. The enzyme concentration that hydrolyzes 50% of the substrate was chosen for each inhibition assay of mutants. The hydrolysis rate has a linear relationship with the enzyme concentration and time until 65% substrate has been converted to product. Each experiment was repeated two or three times. The IC_{50} values are the concentration of inhibitors when 50% activities of the enzymes are inhibited.

2.4. Results

Kinetic properties -- The catalytic domain of PDE7A1 has a K_M value of $0.2 \pm 0.03 \mu\text{M}$ and a k_{cat} value of $1.6 \pm 0.2 \text{ s}^{-1}$ for cAMP (Figure 2.3), in contrast to a K_M of $3.9 \pm 0.7 \text{ mM}$ and a k_{cat} of $6.8 \pm 1.3 \text{ s}^{-1}$ for cGMP (Table 2.3). The ratio of the specificity constants $(k_{cat}/K_M)^{cAMP}/(k_{cat}/K_M)^{cGMP}$ is about $\sim 4,000$. The full length PDE4D2 has K_M of $1.5 \pm 0.2 \mu\text{M}$ and k_{cat} of $3.9 \pm 0.3 \text{ s}^{-1}$ for cAMP and K_M of $1.0 \pm 0.1 \text{ mM}$ and k_{cat} of $5.2 \pm 0.8 \text{ s}^{-1}$ for cGMP. The ratio of the specificity constants $(k_{cat}/K_M)^{cAMP}/(k_{cat}/K_M)^{cGMP}$ is about ~ 500 . Thus, these specific constants confirm that PDE7A1 and PDE4D2 are cAMP specific. The k_{cat} value of our PDE7A1 catalytic domain is about 5 times that of PDE7A1 refolded from the inclusion bodies (11) and about half that of PDE4D2, suggesting that the purified PDE7A1 catalytic domain has a native-like folding. It is interesting to note that both PDE4D2 and PDE7A1 have similar k_{cat} values for cAMP and cGMP. However, the K_M values for cGMP are about 700 and 2000 fold bigger than those for cAMP, thus implicating that K_M is the dominant factor for substrate specificity.

Overall structure of PDE7 -- The catalytic domain of PDE7A1 (residues 130-482) contains 17 α -helices (Figure 2.4) and has the same topology of folding as do other PDEs (15, 19-28). Two divalent metals were tentatively interpreted as Zn and Mg for the purpose of structure refinement. Residues 130-138 and 458-482 were not traceable in the structure due to lack of electron density. The N-terminal fragments of the catalytic domains in the PDE families (130-157 in PDE7A1) do not have comparable amino acid sequences and vary in their secondary structure elements. Among them, PDE4B, PDE4D, and PDE1B (15, 19, 26) contain helices H1 and H2 have a similar folding; PDE3B (28) shows only a comparable helix

H2; and PDE5 and PDE9 have different secondary and tertiary structures for their N-terminal residues (24,25). The catalytic domain of PDE7A1 resembles PDE4 mostly and their entire catalytic domains are comparable, as shown by an average difference of 0.93 Å for the superposition of C α atoms of PDE7A1 residues 139-455 on the equivalents of PDE4D2. However, minor differences are observed between PDE7A1 and PDE4D2. First, PDE7A1 has two deletions around residues 297 and 341 (Figure 2.4C). Second, two 3_{10} helices (a type of helix involving 3 residues/turn) in PDE4D2 appear as α -helices in PDE7A1 (He and H10, Figure 2.4C) and a 3_{10} helix in PDE4D2 (residues 98-102) becomes a coil in PDE7A1. The most significant change is associated with the N-terminal portion of helix H11 (residues 304-310 of PDE7A1), which shows an average positional movement of 2.8 Å, about ~3 times the overall average of 0.93 Å for the whole catalytic domain. This structural change appears to be statistically meaningful, but the biological significance is not clear. The positional change of helix H11 may either reflect intrinsic conformation variation between PDE4 and PDE7 or may be due to the tetramer formation in the PDE4D2 crystal, because H11 contributes a small portion of the interface of the PDE4D2 tetramer but is not involved in lattice packing in PDE7A1.

IBMX binds to a subpocket common for all PDE inhibitors -- IBMX (Figure 2.1) is a non-selective inhibitor for most PDEs and shows IC₅₀ of 2-9 μ M for PDE7A and PDE7B (5, 9, 10). The catalytic domain of PDE7A1 has an IC₅₀ of 8.1 ± 0.4 μ M for IBMX, thus implying that the binding determinants are located within the catalytic domain of PDE7. This argument is supported by the crystal structure of PDE7A1, in which IBMX occupies the bottom of the deep pocket and is not exposed at the surface of the catalytic domain. The xanthine ring of

IBMX stacks against Phe416 (Figure 2.5, Table 2.4) and its oxygen O6 forms a hydrogen bond with Gln413 (Figure 2.5, Table 2.4). It also contacts PDE7A1 residues Tyr211, Val380, and Phe384 via van der Waals' interactions (Figure 2.5, Table 2.4). Two water molecules bound to O2 and N7 of xanthine, respectively (Table 2.4). The isopropanyl group of IBMX interacts with residues Phe384, Ile412, and Phe416 (Figure 2.5, Table 2.4). The above interactions of IBMX with PDE7A1 are similar to those in other PDEs (24,25). Overall, IBMX shows conservation of stacking against phenylalanine and a hydrogen bond to the invariant glutamine in all the PDE families. However, IBMX shows significant positional shifts among PDE4, 5, 7, and 9. For example, IBMX in PDE7A1 has an average positional shift of about 1.3 Å from that in PDE4D2. This may reflect that the large pockets in PDEs allow orientational variation of IBMX, as long as the stacking and the hydrogen bond are conserved. Based on the crystal structures of PDE4, 5, 7 and 9 in complex with IBMX, the hydrogen bond with the invariant glutamine and stacking against the phenylalanine appear to be two key components for common binding of all PDE inhibitors (24, 25). This argument is supported by the studies on the structures of PDE4 and PDE5 in complex with various inhibitors (27).

Insensitivity of PDE7 to PDE4 inhibitors -- Rolipram and its derivatives RO-20-1724 and zardaverine do not significantly inhibit the catalytic domain of the wild-type PDE7A1 (Table 2.5), consistent with reports in the literature (9, 10). PDE7A1 is more sensitive to inhibition by etazolate than by other PDE4 inhibitors, perhaps because etazolate has a structure similar to non-selective inhibitor IBMX (Figure 2.1).

The inhibitor sensitivity can be explained on the basis of the crystal structures of PDE4D2-rolipram and PDE7A1-IBMX. The structure of PDE4D2-rolipram showed that the rolipram binding in PDE4 is stabilized by two hydrogen bonds with the invariant glutamine Gln369, whose conformation is fixed by the hydrogen bond to Tyr329 (15, 20, 27). In PDE7A1, the invariant glutamine Gln413 does not form a hydrogen bond with the Tyr329 equivalent, Ser373, but with Ser377. The structural superposition between the catalytic domains of PDE7A1 and PDE4D2 shows that Gln413 in PDE7A1 exhibits the same side chain conformation as that of Gln369 in PDE4D2 with an average positional shift of 1.1 Å (Figure 2.5C). This positional change is slightly higher than the average difference of 0.93 Å between PDE7A1 and PDE4D2, but is about twice those of other active site residues (e. g. 0.56 Å for Ser373/Tyr329). Thus, the conformation and positioning of the glutamine side chain and the scaffolding residues must be the factors for recognition of inhibitors. On the other hand, Ile412 of PDE7A1, which neighbors on Gln413, has a positional shift of 1.6 Å from its corresponding partner Ser368 in PDE4D2, almost twice the overall average difference. The positional change and variation of amino acid type make a different size and shape of the binding pocket in PDE7A1 from PDE4D2 (Figures 5D and 5E), so that Ile412 may be the third factor for inhibitor selectivity. In fact, modeling of rolipram into PDE7A1 on the basis of the structural superposition shows that the side chain of Ile412 is located less than 1 Å from the cyclopentanyl group of rolipram (Figure 2.5C), indicating that it sterically hinders the binding of rolipram. In summary, the PDE7 structure suggests that at least three factors play roles in inhibitor selectivity: (1) the conformation and positioning of the invariant glutamine (Gln413 in PDE7A1), (2) residues scaffolding the glutamine such as Tyr329 in

PDE4D2 and Ser377 in PDE7A1, and (3) residues affecting the shape and size of the binding pockets such as Ile412 in PDE7A1.

Multiple determinants for inhibitor selectivity -- To further understand the inhibitor selectivity in PDE4 and PDE7, kinetic analysis was carried out on the mutations on residues Ser373, Ser377, and Ile412 of PDE7A1, and Tyr329 of PDE4D2. Single mutations of the PDE7A1 residues to the equivalents of PDE4D2 showed decrease of the IC_{50} values by 2-3 fold for rolipram (Table 2.5, Figure 2.6). Because the changes of IC_{50} values are at least 8-fold that the experimental errors (Table 2.5), the sensitivity increase of the mutants to rolipram inhibition is statistically significant. The double PDE7/4 mutations reduced the IC_{50} values for rolipram by 4-6 fold (Figure 2.6, Table 2.5). The most dramatic change is the S373Y/S377T/I412S triple mutation that showed IC_{50} of 3.2 μ M for (R, S)-rolipram, k_{cat} of 2.7 s^{-1} , and K_M of 2.2 μ M for cAMP. All of the three kinetic parameters are very close to 0.55, 3.9, and 1.5 for the wild type PDE4D2, respectively.

Consistently, the PDE7A1 mutants showed increases of the sensitivity to the other PDE4 inhibitors (Table 2.5). RO-20-1724 had IC_{50} of 245 μ M for the wild type PDE7A1, but the IC_{50} values of the single mutants were reduced by 2-9 fold. The triple mutation exhibited IC_{50} of 5.5 μ M, only about 2 times higher than 2.9 μ M for the wild type PDE4D2. The dual PDE3/4 inhibitor zardaverine showed the IC_{50} values of 75 μ M for wild type PDE7A1, 1.0 μ M for wild type PDE4D2, and 2.3 μ M for the triple mutant of PDE7A1 (Table 2.5). The insensitivity of zardaverine to the I412S mutant of PDE7A1 probably is due to the small fluoride group.

To see whether introduction of a PDE7 residue to PDE4 could make a PDE7-like enzyme, we examine the Y329S mutant of PDE4D2. This single mutation of PDE4D2 resulted in 2-75-fold loss in sensitivity to the PDE4 inhibitors (Figure 2.7, Table 2.5), confirming the importance of the tyrosine residue as the scaffold and also cross-verifying the effects observed in the PDE7A1 mutants. In short, the kinetic data suggest that the three residues must work together to significantly change the inhibitor selectivity.

2.5. Discussion

Extensive structural studies have shed light on the substrate specificity and inhibitor selectivity of PDEs (15, 19-28). The structures of PDE4 in complex with rolipram (15, 20, 27) showed that an invariant glutamine (Glu369 in PDE4D2) forms two hydrogen bonds with rolipram, implying a critical role of the glutamine in inhibitor binding. On the other hand, the opposite orientation of the side chain of the glutamine in the PDE4 and PDE5 structures (24, 26) also suggest a key role of the glutamine in substrate specificity. Comparison of the structures of PDE4, PDE5, and PDE9 in complex with IBMX leads to identification of a common pocket for non-selective binding for all PDE inhibitors (24, 25). The structures of PDE4 and PDE5 in complex with various selective inhibitors support the proposal of the common pocket and identify other subpockets that are important for inhibitor binding (27). The structural and kinetic studies on the mutants in this report quantitatively show the role of several residues, thus a further insight into the inhibitor selectivity.

PDE7 was originally named as a family of “rolipram insensitive PDE”, but it has remained unknown why PDE7 is not sensitive to PDE4 inhibitors. To explain the poor inhibition of PDE7 activity by PDE4 inhibitors, a rolipram-recognition triad (Tyr329, Thr333, and Gln369 in PDE4D2, or Ser373, Ser377, and Gln413 in PDE7A1) was proposed on basis of the crystal structures of PDE4D2 in complex with rolipram(15). The side chain conformation of invariant Gln369 is stabilized by a hydrogen bond to Tyr329 in PDE4. It was also predicted that the replacement of Tyr329 with Ser373 in PDE7A1 would switch the side chain of Gln413 away from Ser373 to form a hydrogen bond with Ser377, thus demolishing the hydrogen bonds between the glutamine and rolipram (15). The PDE7A1-IBMX structure

reveals the hydrogen bond between Gln413 and Ser377, confirming the earlier prediction (15). However, the invariant glutamine (Gln413 in PDE7A1) does not change its side chain conformation but its position, thus suggesting that the positioning of the glutamine is critical for inhibitor binding. In addition, my study shows that two groups of residues are critical for the inhibitor selectivity. One is the scaffolding residues such as Tyr329 in PDE4D2 and Ser377 in PDE7A1, which support the conformation and position of the invariant glutamine. Another is residues such as Ile412 in PDE7A1 that affect the shape and size of the binding pocket.

The significant change of the inhibitor sensitivity by the single mutations of PDE7A1 and PDE4D2 can be explained on a structural basis. The S373Y mutation in PDE7A1 may add a PDE4-like hydrogen bond network between the mutated Tyr373 and Gln413, thus placing the glutamine in a favorable position for formation of hydrogen bonds with rolipram (Figure 2.5C). Similarly, the Y329S mutation in PDE4D2 will release Gln369 from the hydrogen bond and thus disfavor its interaction with rolipram. Although the S377T mutation in PDE7A1 is relatively conserved, modeling of the torsion angles of the threonine shows that C γ of Thr377 blocks its formation of a hydrogen bond with Gln413 so as to release Gln413 for interaction with rolipram. The I412S mutation in PDE7A1 apparently makes room for binding of rolipram and avoids of steric clash (Figure 2.5B). Although the single mutations change the inhibitor sensitivity significantly, none of them produces an engineered enzyme comparable with the wild types. The PDE4D-like behavior of the triple mutant of PDE7A1

suggests that the multiple components must work together to determine the inhibitor selectivity.

The studies in this report provide clues for design of selective inhibitors against PDE4 or PDE7. The subpocket occupied by the cyclopentanyl group of rolipram in PDE4 is filled with or closed up by Ile412 in PDE7. Therefore, the cyclopentanyl group of rolipram or a similar group in a PDE4 selective inhibitor can be designed to occupy this subpocket. In comparison, PDE7 selective inhibitors must have a small group for this pocket to avoid of any clashes. Since both the conformation and position of the invariant glutamine are important for inhibitor binding, a dual-selective inhibitor targeting both PDE4 and PDE7 can be designed by forming hydrogen bonds with the glutamine and stacking against Phe372 in PDE4 or Phe416 in PDE7.

Although each PDE family may have its characteristic components for inhibitor recognition, the three elements (an invariant glutamine, scaffolding residues, and residues affecting the pocket) would play essential roles in inhibitor recognition in all PDE families because of its conservation and critical location. Therefore, the understanding on the inhibitor selectivity of PDE4 and PDE7 would provide a general guideline for design of highly selective inhibitors of PDE families.

FOOTNOTES

The atomic coordinates and structure factors (code 1ZKL) have been deposited in the Protein Data Bank, Research Collaboratory for Structural Bioinformatics, Rutgers University, New Brunswick, NJ (<http://www.rcsb.org/>).

REFERENCES

1. Bloom, T.J., and Beavo, J.A. (1996) *Proc Natl Acad Sci USA*. **93**, 14188-14192.
2. Giembycz, M.A., Corrigan, C.J., Seybold, J., Newton, R., and Barnes, P.J. (1996) *Br. J. Pharmacol.* **118**, 1945-1958.
3. Li, L., Yee, C., and Beavo, J.A. (1999) *Science* **283**, 848-851.
4. Miro, X., Perez-Torres, S., Palacios, J.M., Puigdomenech, P., and Mengod, G. (2001) *Synapse* **40**, 201-214.
5. Lee, R., Wolda, S., Moon, E., Esselstyn, J., Hertel, C., and Lerner, A. (2002) *Cell Signal.* **14**, 277-284.
6. Yang, G., McIntyre, K.W., Townsend, R.M., Shen, H.H., Pitts, W.J., Dodd, J.H., Nadler, S.G., McKinnon, M., and Watson, A.J. (2003) *J. Immunol.* **171**, 6414-6420.
7. Michaeli, T., Bloom, T.J., Martins, T., Loughney, K., Ferguson, K., Riggs, M., Rodgers, L., Beavo, J.A., and Wigler, M. (1993) *J. Biol. Chem.* **268**, 12925-12932.
8. Han, P., Zhu, X., and Michaeli, T. (1997) *J. Biol. Chem.* **272**, 16152-16157.
9. Gardner, C., Robas, N., Cawkill, D., and Fidock, M. (2000) *Biochem. Biophys. Res. Commun.* **272**, 186-192.
10. Hetman, J.M., Soderling, S.H., Glavas, N.A., and Beavo, J.A. (2000) *Proc. Natl. Acad. Sci., USA*. **97**, 472-476.
11. Richter, W., Hermsdorf, T., Kronbach, T., and Dettmer, D. (2002) *Protein Express. Purif.* **25**, 138-148.
12. Wang, H., Liu, Y., Chen, Y., Robinson, H., and Ke, H. (2005) *J. Biol. Chem.* **280**:30949-30955.
13. Otwinowski, Z. and Minor, W. (1997) *Methods Enzymol.* **276**, 307-326.
14. Navaza, J. and Saludjian, P. (1997) *Methods Enzymol.* **276**, 581-594.
15. Huai, Q., Wang, H., Sun, Y., Kim, H.Y., Liu, Y., and Ke, H. (2003) *Structure* **11**, 865-873.
16. Collaborative Computational Project, Number 4. (1994) *Acta Cryst.* **D50**, 760--763.
17. Jones, T.A., Zou, J-Y., Cowan, S.W. and Kjeldgaard, M. (1991) *Acta Cryst.* **A47**, 110-119.

18. Brünger, A.T., Adams, P.D., Clore, G.M., DeLano, W.L., Gros, P., Grosse-Kunstleve, R.W., Jiang, J.S., Kuszewski, J., Nilges, M., Pannu, N.S., Read, R.J., Rice, L.M., Simonson, T., and Warren, G.L. (1998) *Acta Cryst.* **D54**, 905-921.
19. Xu, R.X., Hassell, A.M., Vanderwall, D., Lambert, M.H., Holmes, W.D., Luther, M.A., Rocque, W.J., Milburn, M.V., Zhao, Y., Ke, H., and Nolte, R.T. (2000) *Science* **288**, 1822-1825.
20. Xu, R.X., Rocque, W.J., Lambert, M.H., Vanderwall, D.E., Luther, M.A., and Nolte, R.T. (2004) *J. Mol. Biol.* **337**, 355-365.
21. Lee, M.E., Markowitz, J., Lee, J.O., and Lee, H. (2002) *FEBS Lett.*, **530**, 53-58.
22. Sung, B.J., Hwang, K.Y., Jeon Y.H., Lee, J.I., Heo, Y.S., Kim, J.H., Moon, J., Yoon, J.M., Hyun, Y.L., Kim, E., Eum, S.J., Park, S., Lee, J.O., Lee, T.G., Ro, S., and Cho, J. M. (2003) *Nature* **425**, 98-102.
23. Huai, Q., Colicelli, J., and Ke, H. *Biochemistry* **42**, 13220-13226 (2003).
24. Huai, Q., Liu, Y., Francis, S. H., Corbin, J.D., and Ke, H. (2004) *J. Biol. Chem.* **279**, 13095-13101.
25. Huai, Q., Wang, H., Zhang, W., Colman, R.W., Robinson, H., and Ke, H. (2004) *Proc. Natl. Acad. Sci., USA*, **101**, 9624-9629.
26. Zhang, K.Y., Card, G.L., Suzuki, Y., Artis, D.R., Fong, D., Gillette, S., Hsieh, D., Neiman, J., West, B.L., Zhang, C., Milburn, M.V., Kim, S.H., Schlessinger, J., and Bollag, G. (2004) *Mol. Cell* **15**, 279-286.
27. Card, G.L., England, B.P., Suzuki, Y., Fong, D., Powell, B., Lee, B., Luu, C., Tabrizizad, M., Gillette, S., Ibrahim. P.N., Artis, D.R., Bollag, G., Milburn, M.V., Kim, S.H., Schlessinger, J., and Zhang, K.Y. (2004) *Structure* **12**, 2233-2247.
28. Scapin, G., Patel, S.B., Chung, C., Varnerin, J.P., Edmondson, S.D., Mastracchio, A., Parmee, E.R., Singh, S.B., Becker, J.W., Van der Ploeg, L.H., and Tota, M.R. (2004) *Biochemistry* **43**, 6091-6100.

Figure 2.1. Chemical structures of PDE inhibitors.

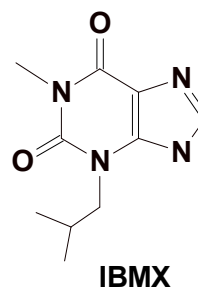
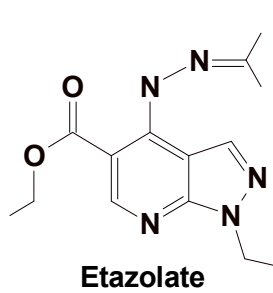
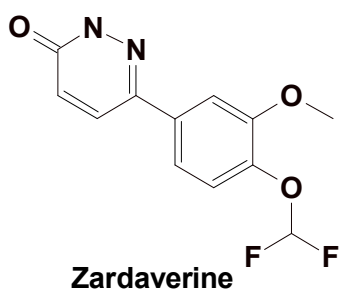
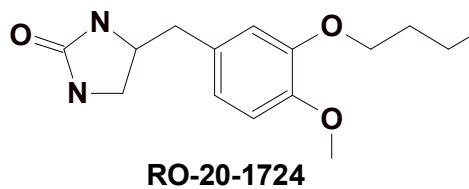
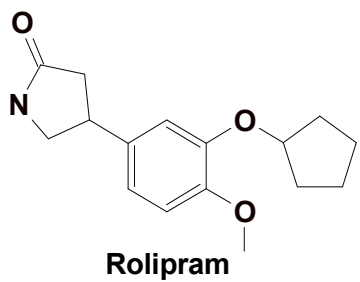


Figure 2.2. The 15% SDS acrylamide gel on the purified proteins. The wild type and mutant Y329S of PDE4D2 are shown in lanes 1 and 2, respectively. The remaining lanes are for PDE7A1 (130-482): wild type (lane 3), S373Y (lane 4), S377T (lane 5), I412S (lane 6), S373Y/S377T (lane 7), S373Y/I412S (lane 8), S377T/I412S (lane 9) and S373Y/S377T/S412S (lane 10).

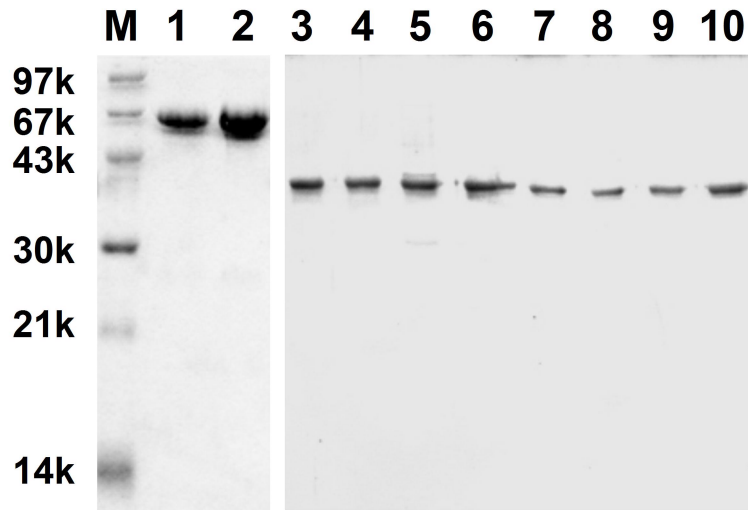
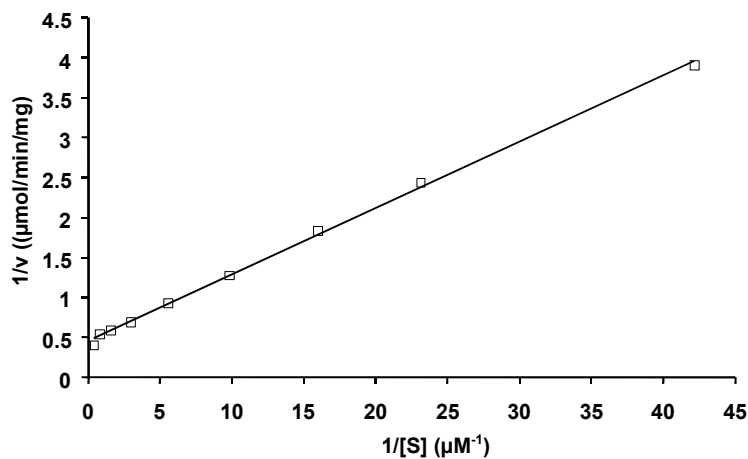
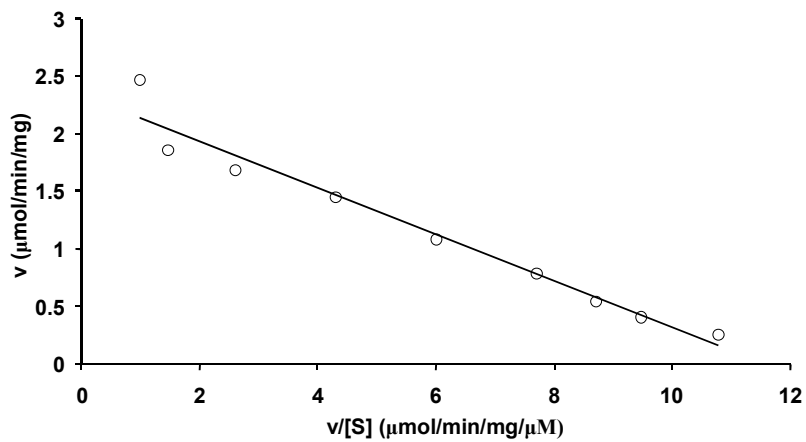


Figure 2.3. PDE7 kinetic. (A) The Lineweaver–Burk plot. The calculated K_M is $0.18 \mu\text{M}$, V_{max} is $2.19 \mu\text{mol}/\text{min}/\text{mg}$. (B) The Eadie-Hofstee plot. The calculated K_M is $0.20 \mu\text{M}$, V_{max} is $2.3 \mu\text{mol}/\text{min}/\text{mg}$. The plots represent the mean of three experiments.

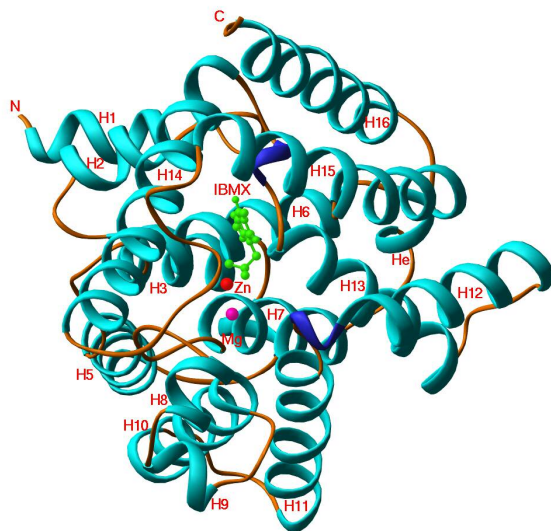


A



B

Figure 2.4. PDE structures. (A) Ribbon diagram of PDE7A1 catalytic domain, IBMX is shown as green balls. Two metals are labeled as Zn and Mg. (B) Ribbons of PDE4D2 catalytic domain. Rolipram is shown as golden balls.



(A)



(B)

Figure 2.4. (C) The alignment of secondary structure and sequence between PDE7A1 and PDE4D2. The three residues that have been mutated are highlighted with yellow.

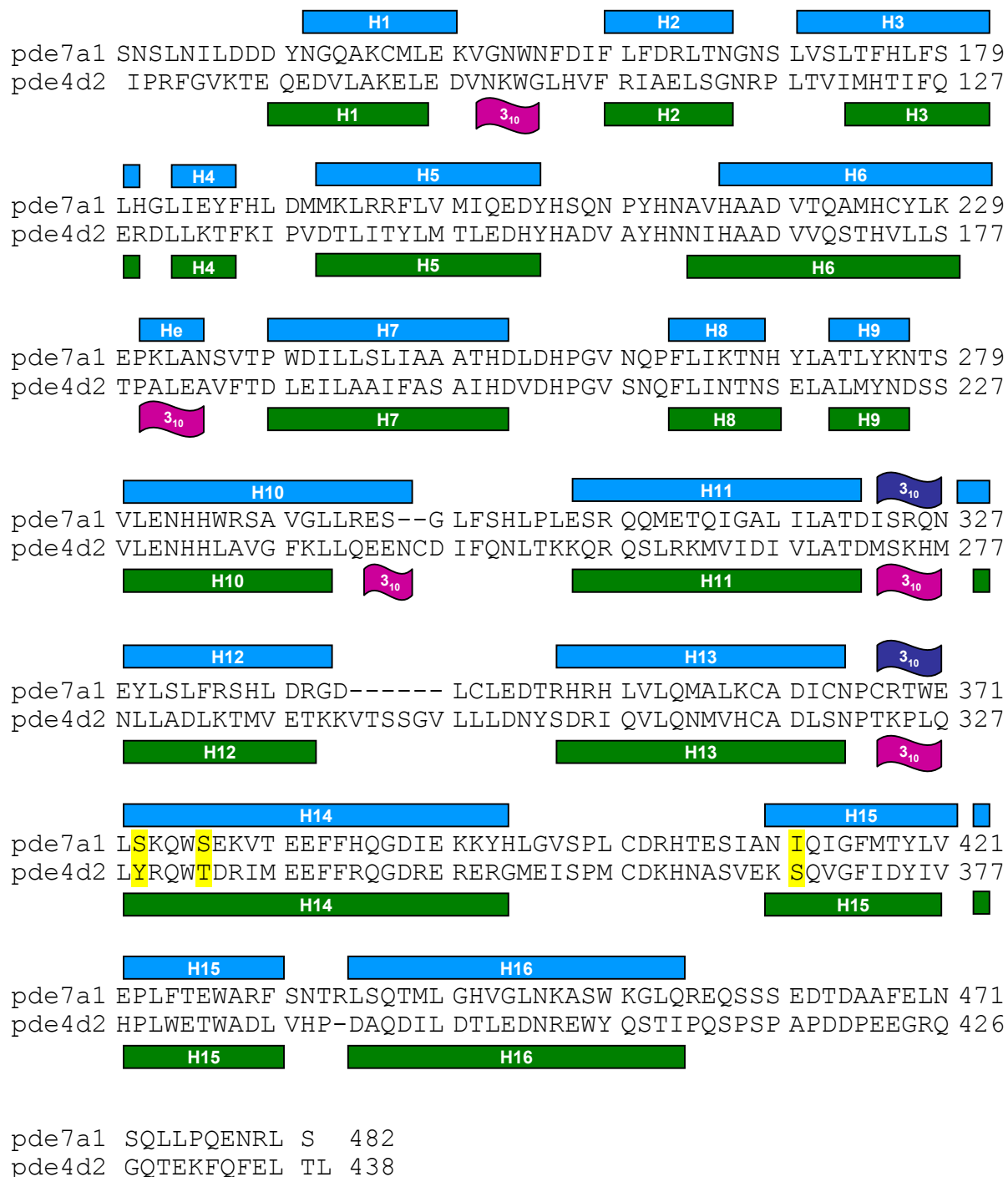
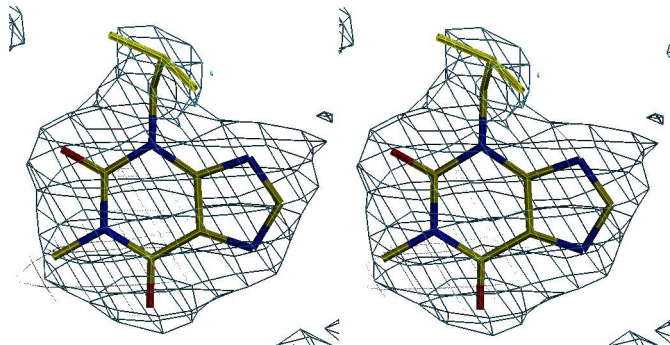
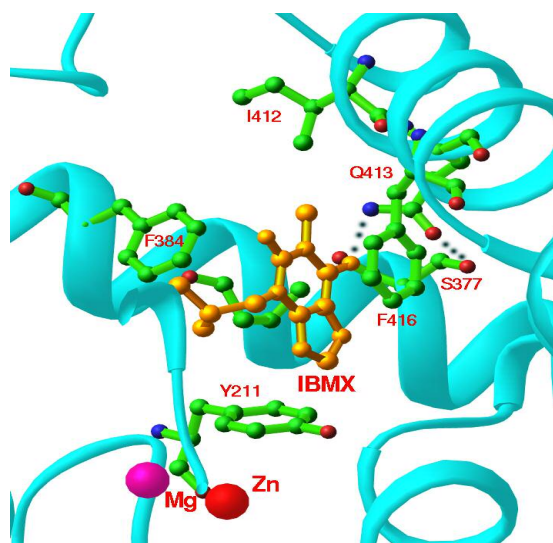


Figure 2.5. The inhibitor binding. (A) Stereo view of electron density for IBMX. The (2Fo-Fc) map was calculated from the structure with omission of IBMX and contoured at 1σ . (B) IBMX (golden sticks-balls) binding to the active site of PDE7A1 catalytic domain. The hydrogen bonds are represented by dotted lines. (C) Superposition of rolipram-binding residues of PDE4D2 (cyan sticks and blue labels) over those of PDE7A1 (green sticks and red labels). The cyclopentanyl ring of rolipram will clash with the side chain of Ile412 if Gln413 forms hydrogen bonds with the oxygen atoms of phenylmethoxy of rolipram. (D) Surface presentation of the subpocket for the cyclopentanyl group of rolipram in PDE4D2. (E) Surface presentation for the same binding pocket in PDE7A1. It is visible that the size and shape of the subpocket for the cyclopentanyl group are different.

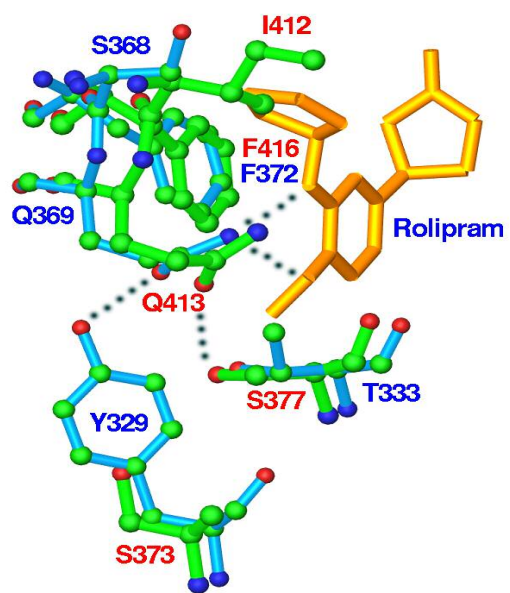
Figure 2.5.



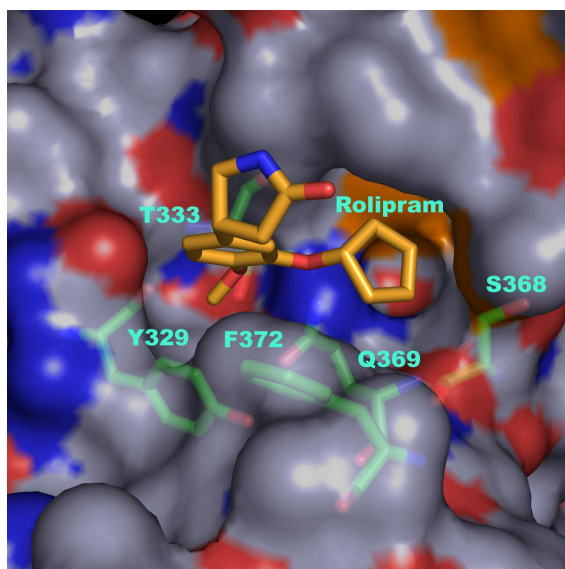
(A)



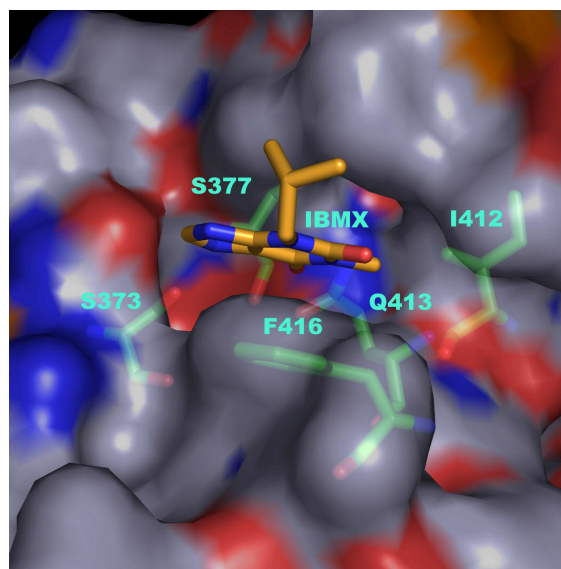
(B)



(C)



(D)



(E)

Figure 2.6. Inhibition on the cAMP activity of the catalytic domain of the wild type PDE7A1 and its mutants by PDE4 inhibitors: (R, S)-rolipram, RO-20-1724, zardaverine, and etazolate. The error bars were calculated from two or three times of repeated measurement.

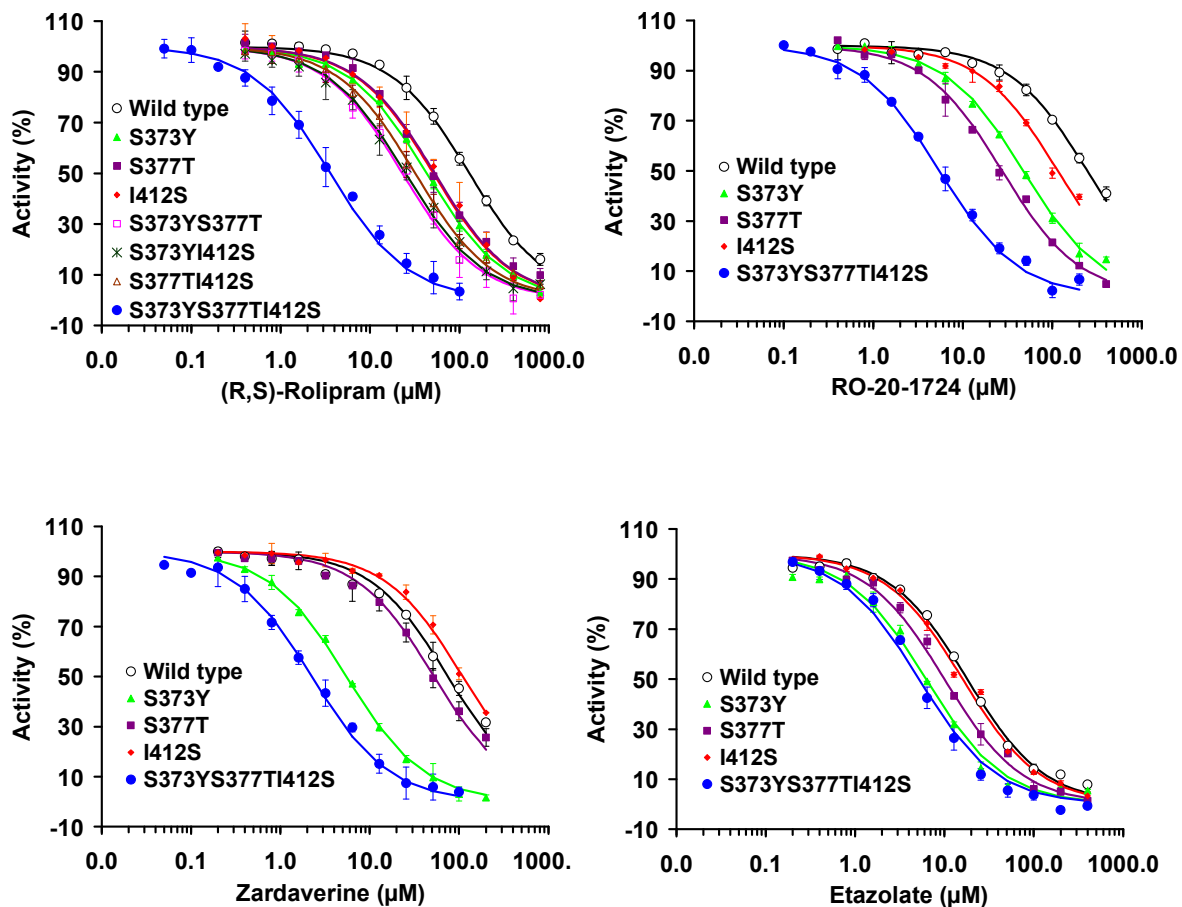


Figure 2.7. Inhibition on the cAMP activity of the wild type PDE4D2 and its Y329S mutant by PDE4 inhibitors: (R, S)-rolipram, RO-20-1724, zardaverine, and etazolate. The error bars were calculated from two or three times of repeated measurement.

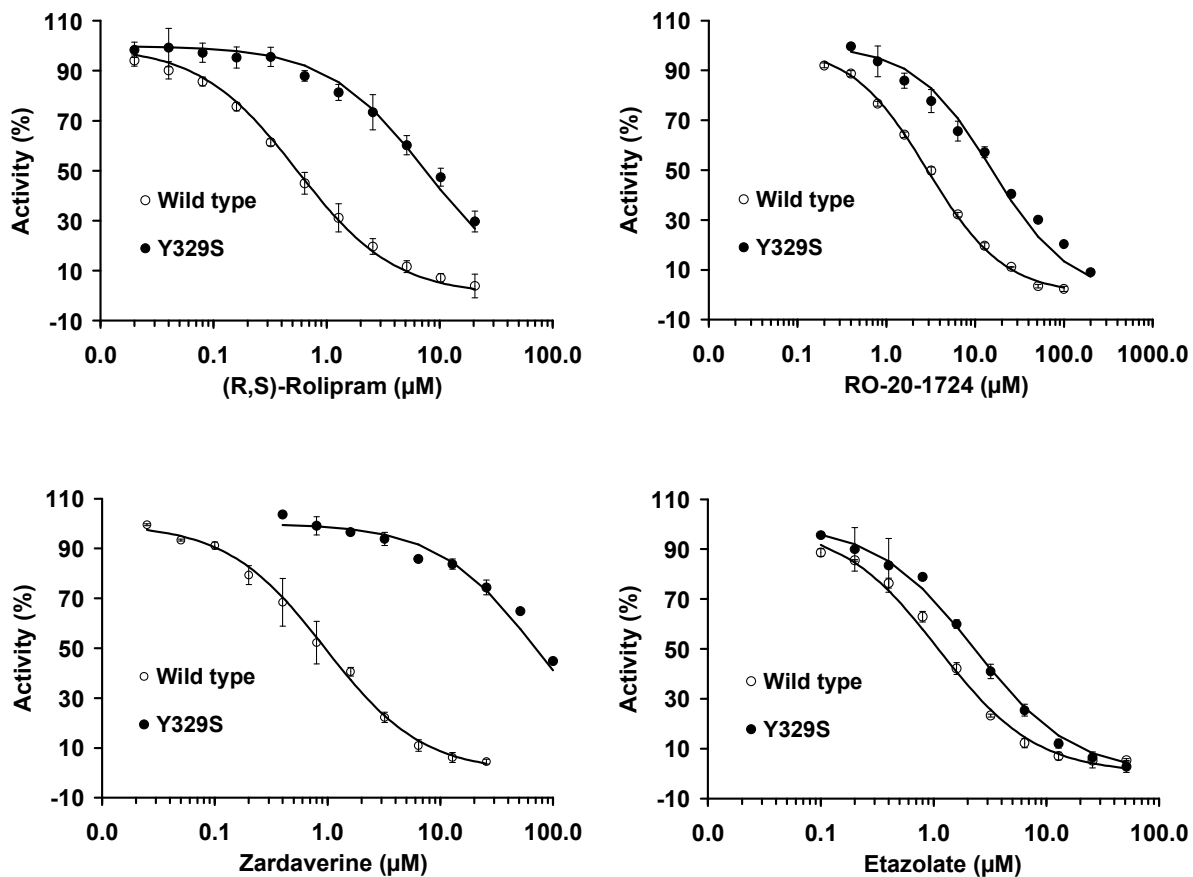


Table 2.1. Primers for mutations of PDE4 and PDE7.

Mutants*	Primers
PDE7A1-S373Y	5' -CCATGTCGGACGTGGGAGCTCTACAAGCAGTGGAGTGAAAAAG and 3' -CTTTTTTCACTCCACTGCTTGTAGAGCTCCCACGTCCGACATGG
PDE7A1-S373Y/S377T**	5' -GTCGGACGTGGGAGCTTTACAAGCAGTGGACTGAAAAAGTAACGGAGG 3' -CCTCCGTTACTTTTTTTCAGTCCACTGCTTGTAAAGCTCCCACGTCCGAC
PDE7A1-S377T	5' -CCATGTCGGACGTGGGAGCTCTCCAAGCAGTGGACTGAAAAAGTAACG 3' -CGTTACTTTTTTTCAGTCCACTGCTTGGAGAGCTCCCACGTCCGACATGG
PDE7A1-I412S	5' -CACACTGAATCTATTGCGAATTCAGATTGGTTTTATGAC 3' -GTCATAAAACCAATCTGGGAATTCGCAATAGATTCAGTGTG
PDE4D2-Y329S	5' -CAACAAAGCCTCTCCAGCTGAGCCGCCAGTGGACGGACC 3' -GGTCCGTCCACTGGCGGCTCAGCTGGAGAGGCTTTGTGG

*For other mutants, PDE7A1-S373Y/I412S, PDE7A1-S377T/I412S and PDE7A1-S373Y/-S377T/I412S were generated from PDE7A1-S373Y, PDE7A1-S377T and PDE7A1-S373Y/S377T using primers of PDE7A1-I412S, respectively.

** Generated from PDE7A1-S373Y.

Table 2.2. Statistics on diffraction data and structure refinement.

<i>Data collection</i>	PDE7A1-IBMX
Space group	P3 ₁ 21
Unit cell (a, b, c, Å)	115.8, 115.8, 64.3
Resolution (Å)	50-1.67 (1.73-1.67)
Total measurements	410,779
Unique reflections	57,579
Completeness (%)	99.6 (96.2)*
Average I/σ	13.2 (2.5)*
Rmerge	0.071 (0.48)*

<i>Structure Refinement</i>	
Resolution (Å)	50-1.67
Reflections	55,766
R-factor/R-free	0.194/0.207

Number of atoms	
Protein	2596
IBMX	16
Waters	289
Zn	1
Mg	1
Average B-factor (Å ²)	
Protein	20.9
IBMX	25.0
Waters	32.7
Zn	15.4
Mg	13.7
RMS deviation for	
Bond	0.005 Å
Angle	1.1°

*The numbers in parentheses are for the highest resolution shell.

Table 2.3. Kinetic Parameters of PDE4D2(1-507) and PDE7A1(130-482).

	K_M^{cAMP} (μM)	k_{cat}^{cAMP} (S^{-1})	$(k_{cat}/K_M)^{cAMP}$ ($\text{S}^{-1}\mu\text{M}^{-1}$)	K_M^{cGMP} (μM)	k_{cat}^{cGMP} (S^{-1})	$(k_{cat}/K_M)^{cGMP}$ ($\text{S}^{-1}\mu\text{M}^{-1}$)	$\frac{(k_{cat}/K_M)^{cAMP}}{(k_{cat}/K_M)^{cGMP}}$
PDE4D2	1.5 \pm 0.2	3.9 \pm 0.3	2.7 \pm 0.4	9.9 \pm 1.0 $\times 10^2$	5.2 \pm 0.8	5.3 \pm 0.8 $\times 10^{-2}$	509
PDE7A1	0.20 \pm 0.03	1.6 \pm 0.2	7.9 \pm 0.9	3.9 \pm 0.7 $\times 10^3$	6.8 \pm 1.3	1.8 \pm 0.5 $\times 10^{-3}$	4389

The apparent K_M and k_{cat} values were determined from Eadie-Hofstee plots of v_0 versus $v_0/[S]$. Each value was measured at least three times. Protein concentrations were measured at O.D. 280 nm normalized by the extinction coefficients. The extinction coefficients and molecular weights were calculated using the program ProtoParam.

Table 2.4. Interactions of IBMX with PDE7A1.

Inhibitor atoms			PDE7 atoms	Distance (Å)
IBMX	O6	...	Gln413 NE2	3.25
IBMX	N7	...	Water 106	2.81
IBMX	O2	...	Water 59	2.91
Van der Waals' contacts:				
Xanthine	N9		Phe416	
	C8		Tyr211, Phe416	
	N7		Tyr211, Phe416	
	C5		Phe416, Val380	
	C4		Phe416	
	N3		Phe416	
	C2		Phe416	
	N1		Phe416, Phe384	
	C6		Phe416	
	O6		Val380, Phe416, Gln413,	
	O2		Phe416	
isopropanyl				
	C10		Phe416, Phe384, Ile412,	
	C11		Phe416	
	C14		Phe384	

Table 2.5. Inhibition of PDE4D2 (1-507) and PDE7A1 (130-482) by PDE4 inhibitors.

	Rolipram (IC ₅₀ μM)	RO-20-1724 (IC ₅₀ μM)	Zardaverine (IC ₅₀ μM)	Etazolate (IC ₅₀ μM)
PDE4D2 Wild Type	0.55±0.05	2.9±0.1	0.95±0.15	1.1±0.1
PDE4D2 Y329S	7.5±1.0	16±1	75±5	2.3±0.2
PDE 7A1 Wild Type	129±10	245±5	75±8	18 ±1
PDE 7A1 S373Y	43±3	48 ±2	5.5±0.1	6.3±0.8
PDE 7A1 S377T	54±6	28±2	53±7	10±1
PDE 7A1 I412S	53±9	115±5	110±10	16±1
PDE 7A1 S373Y/I412S	25±1	N/D	N/D	N/D
PDE 7A1 S373Y/S377T	23±3	N/D	N/D	N/D
PDE 7A1 S377T/I412S	32±4	N/D	N/D	N/D
PDE 7A1 S373Y/S377T/I412S	3.6±0.4	5.5±0.5	2.3±0.2	5.2±0.8

The errors were calculated from two or three times of repeated measurement.

CHAPTER III

MULTIPLE CONFORMATIONS OF PHOSPHODIESTERASE-5: IMPLICATIONS FOR ENZYME FUNCTION AND DRUG DEVELOPMENT

3.1. Abstract

Phosphodiesterase-5 (PDE5) is the target for sildenafil, vardenafil, and tadalafil, which are drugs for treatment of erectile dysfunction. This chapter describes the crystal structures of a fully active catalytic domain of unliganded PDE5A1 and its complexes with sildenafil or icarisisid II. These structures together with the PDE5A1-IBMX complex show that the H-loop (residues 660-683) at the active site of PDE5A1 has four different conformations and migrates 7 to 35 Å upon inhibitor binding. In addition, the conformation of sildenafil reported herein is significantly different from those in the previous structures of chimerically hybridized or almost inactive PDE5. Mutagenesis and kinetic analyses confirm that the H-loop is particularly important for substrate recognition.

3.2. Introduction

Inhibitors of PDEs have been widely studied as therapeutics: cardiotonics, vasodilators, smooth muscle relaxants, antidepressants, antithrombotics, antiasthmatics, and agents for improving cognitive functions such as learning and memory (1-8). Some of the most successful examples of this drug class are the PDE5 inhibitors sildenafil (Viagra®), vardenafil (Levitra®), and tadalafil (Cialis®) that are drugs for treatment of male erectile dysfunction (6). However, side effects such as headache and vision disturbance suggest a need for further study of the molecular basis of the selectivity of PDE5 inhibitors (9).

The previous crystal structures of the catalytic domain of the PDE5-inhibitor complexes showed two different conformations of sildenafil (10-12). However, it remains unknown whether these conformations are biologically relevant because the PDE5 enzyme is either almost inactive in one study (10) or a chimeric hybrid in another study (11,12). In addition, the crystal structure of the catalytic domain of PDE5A1 in complex with the non-selective PDE inhibitor 3-isobutyl-1-methylxanthine (IBMX) showed that the conformation of a segment at the active site (the H-loop) is different from the same segment in PDE4 (13) and in other PDE5 structures (10-12,14). Herein I report the structures of the catalytic domains of human PDE5A1 in the unliganded state and in complex with inhibitors sildenafil and icarisisid II (Figure 3.1). These structures, together with that of PDE5A1-IBMX, reveal four different conformations of the H-loop. In addition, comparison of this PDE5-sildenafil structure with the previously published structures shows significantly different conformations of the methylpiperazine portion of sildenafil. These unique features of the PDE5 catalytic domain

and the sildenafil configuration are key considerations for understanding action of sildenafil and for development of PDE5 inhibitors.

3.3. Experimental procedures

Protein expression and purification of catalytic domain of PDE5A1 -- The cDNA of the catalytic domain of human PDE5A1(residues 535-860) was generated by site-directed mutagenesis of the bovine PDE5A cDNA (13). The coding regions for amino acids 535-860 of PDE5A1 were amplified by PCR and subcloned into the expression vector pET15b. The resultant plasmid pET-PDE5A1 was transferred into *E. coli* strain BL21 (Codonplus) for overexpression. The *E. coli* cell carrying pET-PDE5A1 was grown in LB medium at 37°C to absorption $A_{600} = 0.7$ and then 0.1 mM isopropyl β -D-thiogalactopyranoside was added for further growth at 15°C overnight. The *E. coli* cell was resuspended in ice-cold lysis buffer (20 mM Tris.HCl, pH 8.0, 15 mM imidazole, 50 mM NaCl, 1 mM β -mercaptoethanol, plus protease inhibitor mixture), homogenized, and centrifuged after lysed by French Press. The supernatant was loaded into a Ni-NTA agarose (Qiagen) column equilibrated with lysis buffer. The column was washed with lysis buffer and eluted with 150 mM imidazole. Eluted PDE5A1 protein was digested by thrombin to cleave out the 6 \times His tag. The resulted PDE5A1 was loaded into Q-Sepharose ion exchange column and collected in pass-through fractions while most of unwanted proteins bound to the column. The partial purified PDE5A1 proteins was concentrated and further loaded into Sephacryl S300 (Amersham Biosciences) size exclusive column (95cM \times Φ 2.5cM) and eluted with a buffer of 20 mM Tris.HCl, pH 7.5, 1 mM β -mercaptoethanol , 1 mM EDTA and 50 mM NaCl. The catalytic domain of PDE5A1(535-860) was eluted at the fraction numbers 53-59 (6.5 mL/fractions), which was comparable with molecular weight of a monomer (~38Kd). A typical purification yielded over 10 mg PDE5A1 with a purity >95% as determined by SDS/PAGE from a 2-liter cell culture.

The mutants of PDE5A1 were produced by the standard protocol of site-directed mutagenesis (QuikChange site-directed mutagenesis kit (Stratagene)). For the deletion mutants of $\Delta 663-678$ and $\Delta 661-681$, four glycine residues were inserted as spacer to minimize the disturbance on the three-dimensional structure. Overexpression and purification of the mutants used the same protocols as for the wild type protein.

Enzymatic assay -- Enzymatic activity of the isolated catalytic domains of wild type PDE5A1 and its deletion mutants was assayed by using $^3\text{H-cGMP}$ as substrate in a reaction mixture of 20 mM Tris.HCl, pH 7.8, 1.5 mM DTT, 10 mM MgCl_2 , $^3\text{H-cGMP}$ (40000 cpm/assay) at 24°C for 15 min (15). The reaction was terminated by addition of 0.2 M ZnSO_4 and Ba(OH)_2 . Radioactivity of unreacted $^3\text{H-cGMP}$ in the supernatant was measured by a liquid scintillation counter. The turnover rate was measured at nine concentrations of cGMP and controlled at hydrolysis of 15-40% substrate. Each measurement was repeated three times. For measurement of IC_{50} values, ten concentrations of inhibitors were used at a substrate concentration that was tenth of the K_M and an enzyme concentration that hydrolyzed 50% of substrate.

Crystallization and data collection -- All crystals of PDE5A1 (535-860) were grown by vapor diffusion. The protein drop was prepared by mixing 2 μl protein with 2 μl well buffer. The unliganded PDE5A1 crystal was grown at room temperature against well buffer of 0.2 M MgSO_4 , 0.1 M Tris.base (pH 8.5), 12% PEG 3350, and 2% ethanol. The PDE5A1-sildenafil complex was prepared by mixing 1 mM sildenafil with 15 mg/mL PDE5A1 at 4°C overnight and crystallized against a well buffer of 1.0 M sodium citrate, 2.5% ethanol, 0.1 M HEPES

pH 7.5 at 4°C. The PDE5A1-icarisid II complex was prepared by mixing 2 mM icarisid II with 15 mg/mL protein at 4°C overnight, and crystallized against a well buffer of 0.1 M HEPES (pH 7.5), 12% PEG3350 at room temperature.

The unliganded PDE5A1(535-860) was crystallized in the space group $P3_121$ with cell dimensions of $a = b = 74.7$ and $c = 130.7$ Å. The PDE5A1-sildenafil crystal had the space group $P6_222$ with cell dimensions of $a = b = 164.6$ and $c = 193.1$ Å. The PDE5A1-icarisid II crystal had the space group $P6_122$ with cell dimensions of $a = b = 110.7$ and $c = 106.2$ Å. Beamline X25 at Brookhaven National Laboratory was used for collection of diffraction data of the unliganded PDE5A1, and X29 for PDE5A1-sildenafil and PDE5A1-icarisid II (Table 3.1). All data were processed by program HKL (16).

Structure determination -- The structure of the unliganded PDE5A1 was solved by rigid-body refinement of the PDE5A1 catalytic domain in PDE5A1-IBMX. The structures of PDE5A1 in complex with sildenafil and icarisid II were solved by the molecular replacement program AMoRe (17), using the PDE5A1-IBMX structure without the H-loop and IBMX as the initial model. The rotation and translation searches for the crystal of PDE5A1-icarisid II yielded a correlation coefficient of 0.74 and R-factor of 0.31 for 3054 reflections between 4 to 8 Å resolution. The rotation and translation searches for PDE5A1-sildenafil yielded a correlation coefficient of 0.22 and R-factor of 0.52 for 11612 reflections between 4 to 8 Å resolution for the first molecule, and of 0.39 and 0.41 after the second molecule was added. The electron density map was improved by the density modification package of CCP4 (18).

The atomic model was rebuilt by program O (19) and refined by program CNS (Table 3.1, 20).

3.4. Results

Multiple conformations of the H-loop of PDE5 -- The crystallographic asymmetric units contain one molecule of the catalytic domain in the structures of the unliganded PDE5A1 and the icarisid II complex, but three molecules in PDE5A1-sildenafil structure. The electron density maps showed that the entire catalytic domain in the PDE5A1-icarisid II structure and molecule A in the PDE5A1-sildenafil structure were traceable. However, residues 668-676 of molecules B and C in the PDE5A1-sildenafil crystal and residues 793-807 in the unliganded PDE5A1 lacked electron density and were disordered. The Ramachandran plots showed that the backbone conformations of 90-94% residues in the three structures were located in the most favored regions and no residues were located in the energetically disallowed regions.

The structures of the catalytic domains of the unliganded PDE5A1 (residues 535-860) and its complex with sildenafil or icarisid II consist of 14 common α -helices and a variable H-loop at the active site (Figure 3.2). Structural superposition of the unliganded PDE5A1 over the complexes of PDE5A1-IBMX, PDE5A1-sildenafil, and PDE5A1-icarisid II yielded RMS deviations of 0.29, 0.42, and 0.54 Å for the C α atoms of comparable residues (536-659, 684-787, and 810-860), respectively, suggesting overall structural similarity. However, the H-loop (residues 660-683 on the basis of the structural comparison of 7 PDE families, which are slightly different from the previous assignment of residues 661-676 (13)) adopts four conformations and different tertiary structures in the crystals of the unliganded PDE5A1 and its complexes with IBMX, sildenafil, or icarisid II. In the unliganded PDE5A1 structure, the H-loop contains a few turns, but the majority of its residues exist in coil conformation (Figure 3.2). Binding of IBMX converts the H-loop into two short α -helices at residues 664-667 and

672-676 (Figure 3.2F) and shifts the C α -atoms of the H-loop as much as 7 Å from those in the unliganded structure. In the PDE5-sildenafil structure, the H-loop in molecule A is converted to a turn and a 3_{10} -helix at residues 672-675 and the whole loop migrates as much as 24 Å to cover the active site (Figure 3.2). However, the H-loop in molecules B and C are disordered. The most dramatic change in the H-loop occurs in the structure of PDE5A1-icaridisid II, in which the H-loop contains two β -strands at residues 662-666 and 675-679 (Figure 3.2F) and migrates as much as 35 Å from the position in the unliganded PDE5A1.

To verify that the conformational changes are not due to an artifact of structure determination or crystal packing, electron density maps were calculated and lattice interactions in the various crystal forms were examined. The maps that were calculated from the structure with omission of the H-loop showed solid electron density for almost all residues of the H-loops, thus confirming the true conformational variation in the PDE5A1 structures. This is supported by the fact that B-factors for the H-loops are comparable with or slightly higher than the overall average B-factors for the protein atoms: 48 versus 38 Å² for the unliganded PDE5A1, 61 versus 40 Å² for PDE5A1-IBMX, 33 versus 33 Å² for PDE5A1-icaridisid II, and 38 versus 27 Å² for PDE5A1-sildenafil. In addition, the following facts suggest minor roles of the lattice contacts in the conformational changes of the H-loop. First, the unliganded PDE5A1 and its IBMX complex have the same space group and the similar unit cell parameters ($a = b = 74.7$, $c = 130.7$ Å versus $a = b = 74.5$, $c = 130.1$ Å), but different H-loop conformations. Second, the PDE4 H-loop in the chimeric PDE5 structure is involved in the crystal lattice interactions, but retains its PDE4 conformation (12). Thus, the

dramatic conformational changes of the H-loop must be the consequence of binding of the specific inhibitors.

In addition to variation of the H-loop, minor conformational differences are observed for another active site loop, the M-loop (residues 788-811 on the basis of the structural comparison among 7 PDE families, in comparison to the original assignment of residues 787-812 (13)). Residues 793-807 of the M-loop are not traceable in the structures of the unliganded or IBMX-bound PDE5A1. However, the well-ordered M-loops in the structures of PDE5A1 in complex with sildenafil or icarisd II contain an extra 3_{10} helix and a ten-residue extension of α -helix H14, in addition to the correspondence of a 3_{10} helix to the N-terminal portion of H15 in the unliganded PDE5A1 (Figure 3.2f).

PDE5 shows an apparently unique feature distinct from other PDE families, although the overall topological folding of PDE5A is similar to those of PDE1B (12), PDE2A (21), PDE3B (22), PDE4B and PDE4D (12-14, 23-27), PDE7A (15), and PDE9A (28). The core catalytic domains of PDE1, 2, 3, 4, 7, and 9 (residues 115-411 in PDE4D2), including the H-loop that is composed of two short α -helices (H8 and H9, residues 209-215 and 218-222 in PDE4D2, Figure 3.2f), have a uniform conformation and are superimposable on one another. In contrast, the H-loop of PDE5A1 shows four conformations, and none of these is comparable with any of the corresponding H-loops in other PDE families. The closest comparable conformation is the H-loop in the PDE5A1-IBMX structure, which also contains two short α -helices. However, these two helices have as much as 7 Å positional difference from those in PDE4D2 (13), and are in a different three-dimensional arrangement. In

addition, the β -strand components of the H-loop in the PDE5A1-icarisid II complex are unique among active sites of known PDE structures. Therefore, the active site of PDE5 appears to belong to a special category of the PDE superfamily.

Conformation variation of sildenafil -- Sildenafil binds to each active site of three PDE5A1 catalytic domains in the crystallographic asymmetric unit with similar conformation and occupancy, as shown by the comparable B-factors and the clean electron density in the omitted maps (Figure 3.3). The binding of sildenafil causes a dramatic conformational change of the H-loop and a movement as much as 24 Å from that in the unliganded PDE5 structure. A direct consequence of the H-loop movement is the transformation of the open PDE5A1 active site to a closed pocket. Sildenafil is partially buried in the pocket. Solvent accessible surface of sildenafil after binding to PDE5A1 is reduced to 9.4% of the total surface area. Sildenafil borders the metal-binding pocket, but does not directly interact with the metal ions. The pyrazolopyrimidinone group (R_1 in Figure 3.1, Table 3.2) of sildenafil stacks against Phe820 of PDE5A1 and also contacts residues Tyr612, Leu765, Ala767, and Gln817. The O1 and N4 atoms of pyrazolopyrimidinone form two hydrogen bonds with NE2 and OE1 of Gln817, respectively. The ethoxyphenyl group (R_2 , Figure 3.1) interacts via van der Waals forces with Val782, Ala783, Phe786, Leu804, Ile813, Gln817, and Phe820. The methylpiperazine group (R_3 , Figure 3.1) contacts Asn662, Ser663, Tyr664, Ile665, Leu804, and Phe820. The oxygen atoms of the sulfate group interact mainly with Phe820.

Our PDE5A1-sildenafil structure is similar in many respects to those reported earlier (10-12), as shown by the RMS deviations of 0.59 and 0.40 Å for superposition of the

backbone atoms of the comparable residues (without 661-677) of our PDE5A1-sildenafil over the two previous structures. However, two significant differences are observed among the three PDE5A-sildenafil structures. First, the H-loop in our structure has definite electron density and different conformation from those in the previously published structures in which the H-loop is either disordered (missing residues 665-675) (10) or takes the PDE4 conformation due to chimeric replacement of PDE5 residues 658-681 with those of PDE4 (12). Second, the conformations and the interactions of sildenafil in the three PDE5A-sildenafil structures are significantly different. While the ethoxyphenyl and pyrazolopyrimidinone groups of sildenafil in the three PDE5A structures are superimposable and interact with the same residues of PDE5A, the methylpiperazine shows different orientations (Figure 3.3). Methylpiperazine in our PDE5A1-sildenafil structure folds to interact with pyrazolopyrimidinone, in comparison with the conformation that extends in a different direction in the structure of Sung et al. (10). The conformation of the methylpiperazine in the structure of Zhang et al. (12) is similar to ours, but shows a twist of about 40° (Figure 3.3). In addition, the contacts between the methylpiperazine and the H-loop residues differ substantially. In our structure, the methylpiperazine interacts with Asn662, Ser663, Tyr664, and Ile665 in the H-loop (Table 3.2). However, there are no contacts between the methylpiperazine and the H-loop in the structure of Zhang et al., and the methylpiperazine contacts Tyr664, Met816, Gly819, and Phe820 in the structure by Sung et al.

To exclude possible false results from the structure determination, we re-examined the three structures of the PDE5A catalytic domain in complex with sildenafil. The (2Fo – Fc)

and (Fo – Fc) maps that are calculated from the PDE5A catalytic domains with omission of sildenafil show reasonable electron density for all three sildenafil, suggesting their true bound conformations in the crystal states. Thus, the basis for the conformational differences of sildenafil needs to be explored. The difference in twist of about 40° of the methylpiperazine ring may be the consequence of chimeric replacement of the PDE5 H-loop (residues 658-681) with the equivalents of PDE4 in the structure of Zhang et al. (12), in which the H-loop takes the conformation of PDE4. For the structure of PDE5A-sildenafil of Sung et al. (10), the electron density maps show that Cys677 probably forms an intermolecular disulfide bond with Cys677 from a neighboring monomer in the PDE5A crystal. Thus, the catalytic domain of PDE5A in the structure of Sung et al. (10) physically forms a dimer, in contrast to a monomeric form in the PDE5A-sildenafil structures of ours and Zhang et al. (12). The fact that the specific activity of the catalytic domain of Sung et al. (19) is only about one thousandth of that reported for monomeric PDE5A (29 and this study) suggests that the dimer may be either a less active form of PDE5 or a biologically irrelevant artifact. It is interesting to note that the activity of PDE5A was increased 5-10 folds in the presence of reducing agents such as dithiothreitol and β-mercaptoethanol (Figure 3.4). Mutation of Cys677 to aspartic acid (corresponding residue in PDE4) resulted in loss of this effect, implying that the intermolecular disulfide bond formed by Cys677 involved in the conformation changes of the H-loop and therefore affect the enzyme function of PDE5A1. Although there are 9 cysteine residues in the catalytic domain of PDE5, most of them except the Cys677 residue are buried and no disulfide bond has been reported across all PDE families. Whether the disulfide bond observed in the structure of PDE5A-sildenafil of Sung et. al. is biological relevant or not

remains unclear. However, it might indicate that the H-loop may be involved in the regulation of PDE5 activity.

Binding of icarisid II to PDE5 -- Icarisid II is a glycoside derivative of flavonoids from the plant *Epimedium wanshanense* that has been used as an herbal medicine for improvement of erectile dysfunction in China for more than a thousand years (30-33). Icarisid II inhibits PDE5A1 with an IC₅₀ of 2 μM and shows at least 10 fold selectivity against other PDEs. It binds to the active site of PDE5A1, as shown by the electron density that is calculated from the PDE5A1 structure before icarisid II was built in (Figure 3.5). The binding of icarisid II causes formation of two β-strands in the H-loop and as much as 35 Å movement of the H-loop to completely close the active site (Figures 2e & 4). The solvent accessible area of icarisid II after binding to the active site of PDE5A1 is reduced to 0.05% of the unbound form.

Five hydrogen bonds are formed between icarisid II and PDE5A1 residues. The oxochromone (R₂, Figure 3.1, Table 3.2) of icarisid II stacks against Phe820 and its oxygen atoms O4 and O10 form three hydrogen bonds with the backbone nitrogen of Ile665, the side chain oxygen of Ser668, and a water molecule. It also interacts with residues Tyr664, Leu725, Leu804, and Met816 (Figure 3.5). The methoxyphenyl group (R₁, Figure 3.1) forms a hydrogen bond with the backbone nitrogen of Ile768 and makes van der Waals contacts with Ala767, Ile768, Gln775, Ala779, Gln817, and Phe820 (Table 3.2). The pentenyl group (atoms C17-C21, Figure 3.1) forms hydrophobic contacts with Val782, Phe786, Leu804, Met816, and Gln817. The rhamnose group (R₃, Figure 3.1) forms three hydrogen bonds with NE2 of His613, OD2 of Asp764, and a water molecule, in addition to interactions with residues Tyr612, His613, Asn661, Ser663, Leu725, Asp764, Leu765, and Phe820 (Table 3.2). A few

atoms of rhamnose are located at distance suitable for van der Waals' contact with both metal ions and directly interact with the metal-binding residues such as Asp764.

Although icarisisid II and sildenafil occupy the same active site, the detailed interactions of the inhibitors are significantly different (Figure 3.5). Sildenafil forms two hydrogen bonds with Gln817 and stack against Phe820. However, Gln817 shows about 90° rotation of its side chain (Figure 3.5) and forms no hydrogen bond with icarisisid II. In addition, the position of oxchromone of icarisisid II, which stacks against Phe820, is significantly different from the pyrazolopyrimidinone of sildenafil. In consideration of the 1000-fold difference in binding affinity between sildenafil and icarisisid II, the structural data suggest that the hydrogen bond with Gln817 and the stacking with Phe820 are two essential components for high affinity binding of inhibitors.

A potential role of the H-loop in substrate/inhibitor recognition -- To understand the biochemical basis of multiple conformations of the H-loop, two deletion mutants were created in the isolated catalytic domain of PDE5A1. The PDE5A1 mutant with deletion of residues 663-678 and insertion of four glycines (to minimize disturbance of the structure) showed about 10- and 2-fold lower affinity for cGMP and the inhibitors, respectively (Table 3.3, Figure 3.6). The mutant with deletion of residues 661-681 and insertion of four glycines had a 150-fold weaker K_M for cGMP and 30-80-fold less potent IC_{50} for the inhibitors (Table 3.3). However, both mutants had k_{cat} values comparable with that of the wild type PDE5A1 catalytic domain. These data imply that the H-loop is less critical for binding of inhibitors than for cGMP. This is consistent with the early report that a sildenafil homolog UK-122764

that lacks methylpiperazine and thus interactions with the H-loop shows only a 5-fold lower potency than sildenafil (34).

The kinetic data indicate that the $\Delta 663-678$ mutant affects K_M for cGMP, but have much less effect in catalytic turnover rate and inhibitor binding (Table 3.3). Although no interactions between the H-loop and the low affinity product GMP were observed in the chimeric PDE5-GMP structure (12), it is plausible that the H-loop may contact cGMP in a pattern like that of sildenafil or icarisid II. Since hydrolysis of the phosphodiester bond of cGMP occurs in the metal-binding subpocket, the distal position of the H-loop from the metal site in the structure would be more consistent with its role in substrate binding rather than hydrolysis. This would imply a dynamic interplay between the H-loop and substrate, in which binding of cGMP and the H-loop conformation would mutually regulate one another. Further structural studies will be required to completely define the mechanism involved in the H-loop modulation of substrate affinity and inhibitor binding.

3.5. Discussion

Extensive studies on the crystal structures of PDEs have shown that the PDE families have similar three-dimensional structures for their isolated catalytic domains and active sites (19-24, 31-38). However, information on the conformation of the PDE5 active site and on sildenafil binding is incomplete because early studies showed a disordered or artificially replaced H-loop at the active site (10-12). The present study, in combination with the PDE5A1-IBMX structure (13), reveals that the H-loop of PDE5 can adopt four clearly defined conformations. These different conformations of the H-loop of PDE5 may be the result of direct contacts between the H-loop and inhibitors, such as those in the structures of PDE5A1 in complex with sildenafil or icarisid II. Alternatively, the H-loop changes may be imposed by more distant effects of conformational changes following inhibitor occupation of the binding pocket, as implicated by no direct contacts between the H-loop and IBMX. Finally, a combination of both direct and indirect interactions may contribute to the H-loop changes. Since all other PDEs appear to have a similar conformation of the H-loop that is not comparable with any of the conformations of the PDE5 H-loop, the PDE5 active site apparently has a unique structural characteristic. The mutual communication between inhibitor binding and conformational changes of the PDE5 catalytic pocket may thus be valuable for design of new inhibitors with unique selectivity against PDE5.

It is common that an inhibitor slightly adjusts its conformation to provide an optimal fit in the binding pocket of a protein. However, the conformational variation of sildenafil in the different crystal forms, as seen in the significantly different conformations of the methylpiperazine group is unusual. Since inhibitors are commonly designed to mimic

contacts employed by the substrate, the dramatic effect of the H-loop mutations on affinity for cGMP and the flexibility of sildenafil provide potentially important direction in development of new PDE5 inhibitors.

Side effects such as vision disturbance of patients after ingestion of PDE5 inhibitors (9) dictate a need for detailed study of the molecular basis for the action of these drugs and development of new potential inhibitors. Derivatives of flavonoids may be such a new category of PDE5 inhibitors. Flavonoids inhibit PDEs with affinity at the micromolar level and slight selectivity (35,36), and are widely used as dietary supplements that have reached a multiple billion dollar business (37-39). In the present report, the structure of PDE5A1-icarisid II shows how this natural dietary compound interacts with PDE5 and thus provides a valuable guideline for development of a new category of PDE5 inhibitors.

REFERENCES

1. Movsesian, M.A. (2000) *Expert Opin. Investigational Drugs* **9**, 963-973
2. Truss, M.C., Stief, C.G., Uckert, S., Becker, A.J., Wafer, J., Schultheiss, D., and Jonas, U. (2001) *World J. Urol.* **19**, 344-350
3. Liu, Y., Shakur, Y., Yoshitake, M., and Kambayashi, J.J. (2001) *Cardiovascular Drug Rev.* **19**, 369-386
4. Huang, Z., Ducharme, Y., MacDonald, D., and Robinchaud, A. (2001) *Curr. Opin. Chem. Biol.* **5**, 432-438
5. Rotella, D.P. (2002) *Nature Rev. Drug Discovery* **1**, 674-682
6. Corbin, J.D., and Francis, S.H. (2002) *Int. J. Clin. Pract.* **56**, 453-459
7. Lipworth, B.J. (2005) *Lancet.* **365**, 167-175
8. Castro, A., Jerez, M.J., Gil, C., and Martinez, A. (2005) *Med. Res. Rev.* **25**, 229-244
9. Pomeranz, H.D., and Bhavsar, A.R. (2005) *J. Neuroophthalmol.* **25**, 9-13
10. Sung, B.J., Hwang, K.Y., Jeon, Y.H., Lee, J.I., Heo, Y.S., Kim, J.H., Moon, J., Yoon, J.M., Hyun, Y.L., Kim, E., Eum, S.J., Park, S.Y., Lee, J.O., Lee, T.G., Ro, S., and Cho, J.M. (2003) *Nature* **425**, 98-102
11. Brown, D.G., Groom, C.R., Hopkins, A.L., Jenkins, T.M., Kamp, S.H., O'Gara, M.M., Ringrose, H.J., Robinson, C.M., and Taylor, W.E. (2003) WO 2003038080 A1 20030508 CAN 138:364748 AN 2003:356596 CAPLUS: 442
12. Zhang, K.Y., Card, G.L., Suzuki, Y., Artis, D.R., Fong, D., Gillette, S., Hsieh, D., Neiman, J., West, B.L., Zhang, C., Milburn, M.V., Kim, S.H., Schlessinger, J., and Bollag, G. (2004) *Mol Cell.* **15**, 279-286
13. Huai, Q., Liu, Y., Francis, S.H., Corbin, J.D., and Ke, H. (2004a) *J. Biol. Chem.* **279**, 13095-13101
14. Card, G.L., England, B.P., Suzuki, Y., Fong, D., Powell, B., Lee, B., Luu, C., Tabrizizad, M., Gillette, S., Ibrahim, P.N., Artis, D.R., Bollag, G., Milburn, M.V., Kim, S.H., Schlessinger, J., and Zhang, K.Y. (2004) *Structure* **12**, 2233-2247
15. Wang, H., Liu, Y., Chen, Y., Robinson, H., and Ke, H. (2005) *J. Biol. Chem.* **280**, 30949-30955
16. Otwinowski, Z., and Minor, W. (1997) *Methods Enzymol.* **276**, 307-326

17. Navaza, J., and Saludjian, P. (1997) *Methods Enzymol.* **276**, 581-594
18. Collaborative Computational Project, Number 4. (1994) *Acta Cryst.* **D50**, 760-763
19. Jones, T.A., Zou, J-Y., Cowan, S.W., and Kjeldgaard, M. (1991) *Acta Cryst.* **A47**, 110-119
20. Brünger, A.T., Adams, P.D., Clore, G.M., DeLano, W.L., Gros, P., Grosse-Kunstleve, R.W., Jiang, J.S., Kuszewski, J., Nilges, M., Pannu, N.S., Read, R.J., Rice, L.M., Simonson, T., and Warren, G.L. (1998) *Acta Cryst.* **D54**, 905-921
21. Iffland, A., Kohls, D., Low, S., Luan, J., Zhang, Y., Kothe, M., Cao, Q., Kamath, A.V., Ding, Y.H., and Ellenberger, T. (2005) *Biochemistry* **44**, 8312-8325
22. Scapin, G., Patel, S.B., Chung, C., Varnerin, J.P., Edmondson, S.D., Mastracchio, A., Parmee, E.R., Singh, S.B., Becker, J.W., Van der Ploeg, L.H., and Tota, M.R. (2004) *Biochemistry* **43**, 6091-6100
23. Xu, R.X., Hassell, A.M., Vanderwall, D., Lambert, M.H., Holmes, W.D., Luther, M.A., Rocque, W.J., Milburn, M.V., Zhao, Y., Ke, H., and Nolte, R.T. (2000) *Science* **288**, 1822-1825
24. Xu, R.X., Rocque, W.J., Lambert, M.H., Vanderwall, D.E., Luther, M.A., and Nolte, R.T. (2004) *J. Mol. Biol.* **337**, 355-365
25. Lee, M.E., Markowitz, J., Lee, J.O., Lee, H. (2002) *FEBS Lett.* **530**, 53-58
26. Huai, Q., Wang, H., Sun, Y., Kim, H.Y., Liu, Y., and Ke, H. (2003) *Structure* **11**, 865-873
27. Huai, Q., Colicelli, J., and Ke, H. (2003) *Biochemistry* **42**, 13220-13226
28. Huai, Q., Wang, H., Zhang, W., Colman, R., Robinson, H., and Ke, H. (2004b) *Proc. Natl. Acad. Sci. USA*, **101**, 9624-9629
29. Fink, T. L., Francis, H., Beasley, A., Grimes, K. A., and Corbin, J. D. (1999) *J. Biol. Chem.* **274**, 24613-24620
30. Li, W.K., Zhang, R.Y., and Xiao, P.G. (1996) *Phytochemistry* **43**, 527-530
31. Kuroda, M., Mimaki, Y., Sashida, Y., Umegaki, E., Yamazaki, M., Chiba, K., Mohri, T., Kitahara, M., Yasuda, A., Naoi, N., Xu, Z.W., and Li, M.R. (2000) *Planta Med.* **66**, 575-577
32. Xin, Z., Kim, E., Tian, Z., Lin, G., and Guo, Y. (2001) *Chinese Sci. Bulletin* **46**, 1186-1190

33. Xin, Z., Kim, E.K., Lin, C.S., Liu, W.J., Tian, L., Yuan, Y.M., and Fu, J. (2003) *Asian J. Androl.* **5**, 15-18
34. Turko, I.V., Ballard, S.A., Francis, S.H., and Corbin, J.D. (1999) *Mol Pharmacol.* **56**, 124-130
35. Nichols, M.R., and Morimoto, B.H. (2000) *Mol. Pharmacol.* **57**, 738-754
36. Ko, W., Shih, C., Lai, Y., Chen, J., and Huang, H. (2004) *Biochem. Pharmacol.* **68**, 2087-2094
37. Barnes, S., Boersma, B., Patel, R., Kirk, P.M., Darley-Usmar, V.M., Kim, H., and Xu, J. (2000) *BioFactors* **12**, 209-215
38. Fitzpatrick, .L.A. (2004) *Maturias* **44**, S21-S29
39. Limer, J., and Speirs, V. (2004) *Breast Cancer Res.* **6**, 119-127

Figure 3.1. Chemical structures of PDE5 inhibitors. The letters R₁-R₃ label the main groups in sildenafil and icaridisid II. In sildenafil, R₁ represents the pyrazolopyrimidinone group, R₂ is ethoxyphenyl, and R₃ is methylpiperazine. In icaridisid II, R₁ represents the methoxyphenyl group, R₂ is oxochromone, and R₃ is rhamnose.

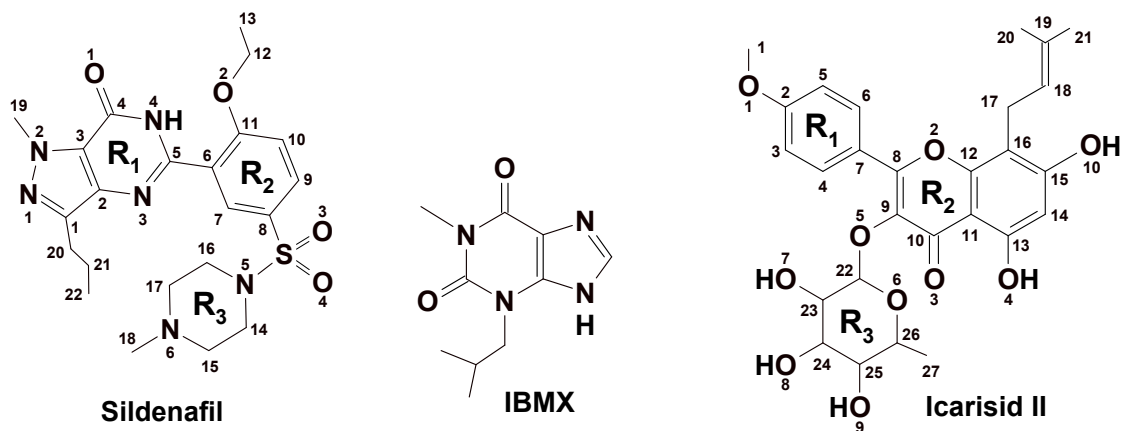

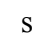

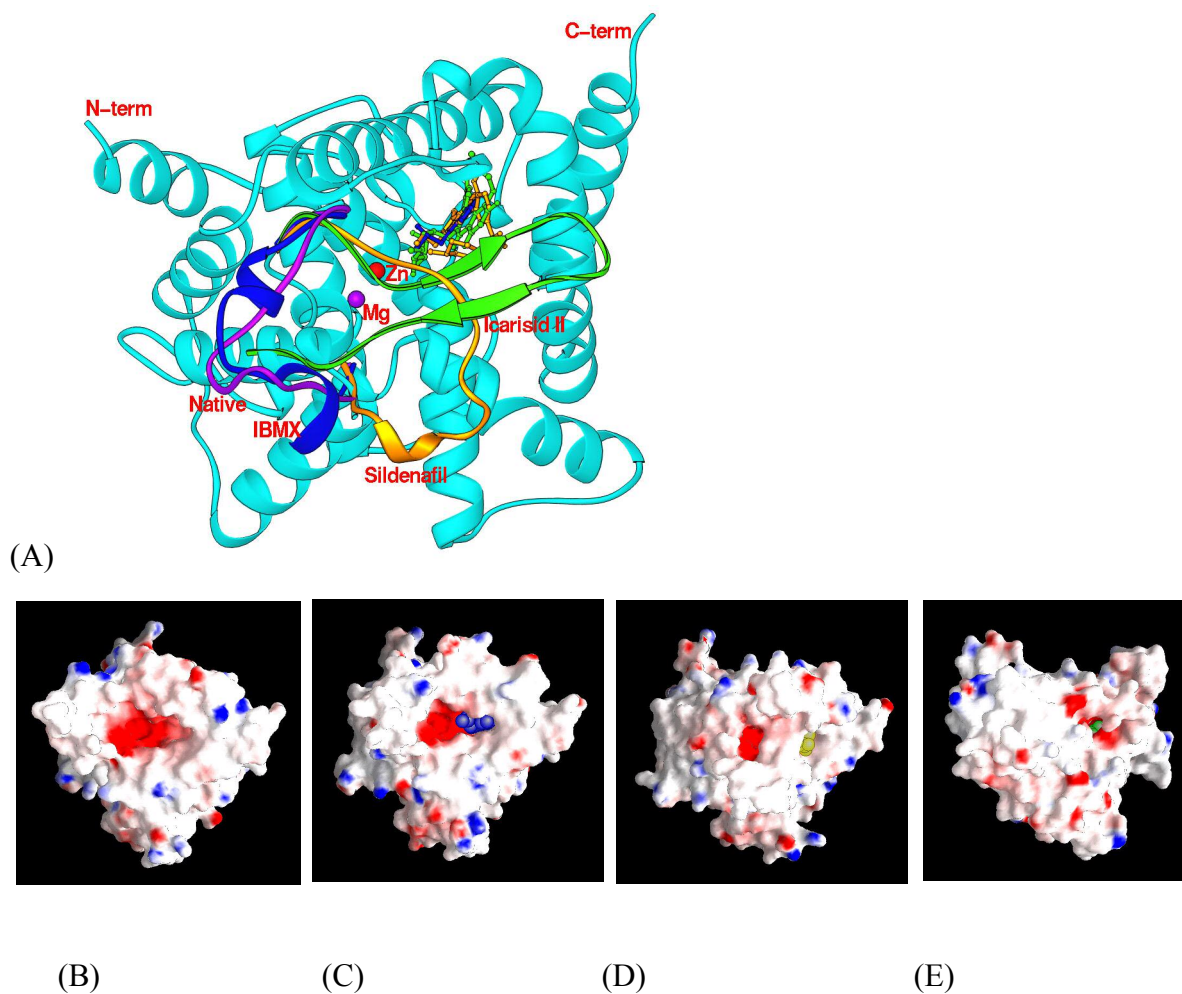
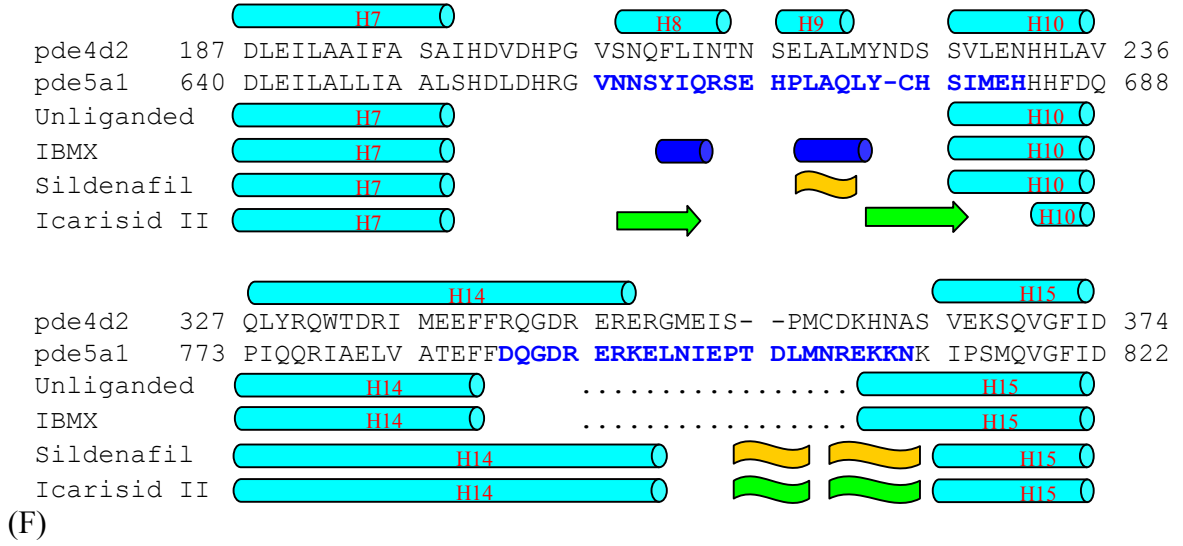


Figure 3.2. Structures of PDE5 and its inhibitor complexes. (A) Ribbon diagram. The cyan ribbons are the common structures of the catalytic domains of unliganded PDE5A1 and its complexes. The different conformations of the H-loop in the four structures are shown in colors of purple for the unliganded PDE5A1, blue for the IBMX complex, golden for the sildenafil complex, and green for the icaridisid II complex. Zn is colored red and Mg is purple. (B)-(E) Surface presentation for the unliganded PDE5A1 catalytic domain (B), PDE5A1-IBMX (C), PDE5A1-sildenafil (D), and PDE5A1-icaridisid II (E). The middle red pocket is the active site. The inhibitors are shown in color balls: blue for IBMX, golden for sildenafil, and green for icaridisid II. Icaridisid II is almost completely buried and the orientation of the domain is adjusted to show up the icaridisid II binding. (F) The alignment of the secondary structures with the amino acid sequence around the regions of the H- and M-loops that are shown in bold letters. The  symbol represents 3_{10} helix;  is for β strand; and  is for α -helix. The dots represent disordered regions in the unliganded and IBMX-bound PDE5.





(F)

Figure 3.3. Sildenafil binding. (A) Stereoview of electron density for sildenafil bound to PDE5A1. The $(2F_o-F_c)$ maps was calculated from the structure omitting sildenafil and contoured at 1.5σ . (B). Interactions of sildenafil (golden stick-balls) with the active site residues (green sticks). The dotted lines represent hydrogen bonds. (C) Superposition of sildenafil from the PDE5A1-sildenafil structures of Zhang et al. (12, golden), Sung et al. (10, cyan), and ours (green).

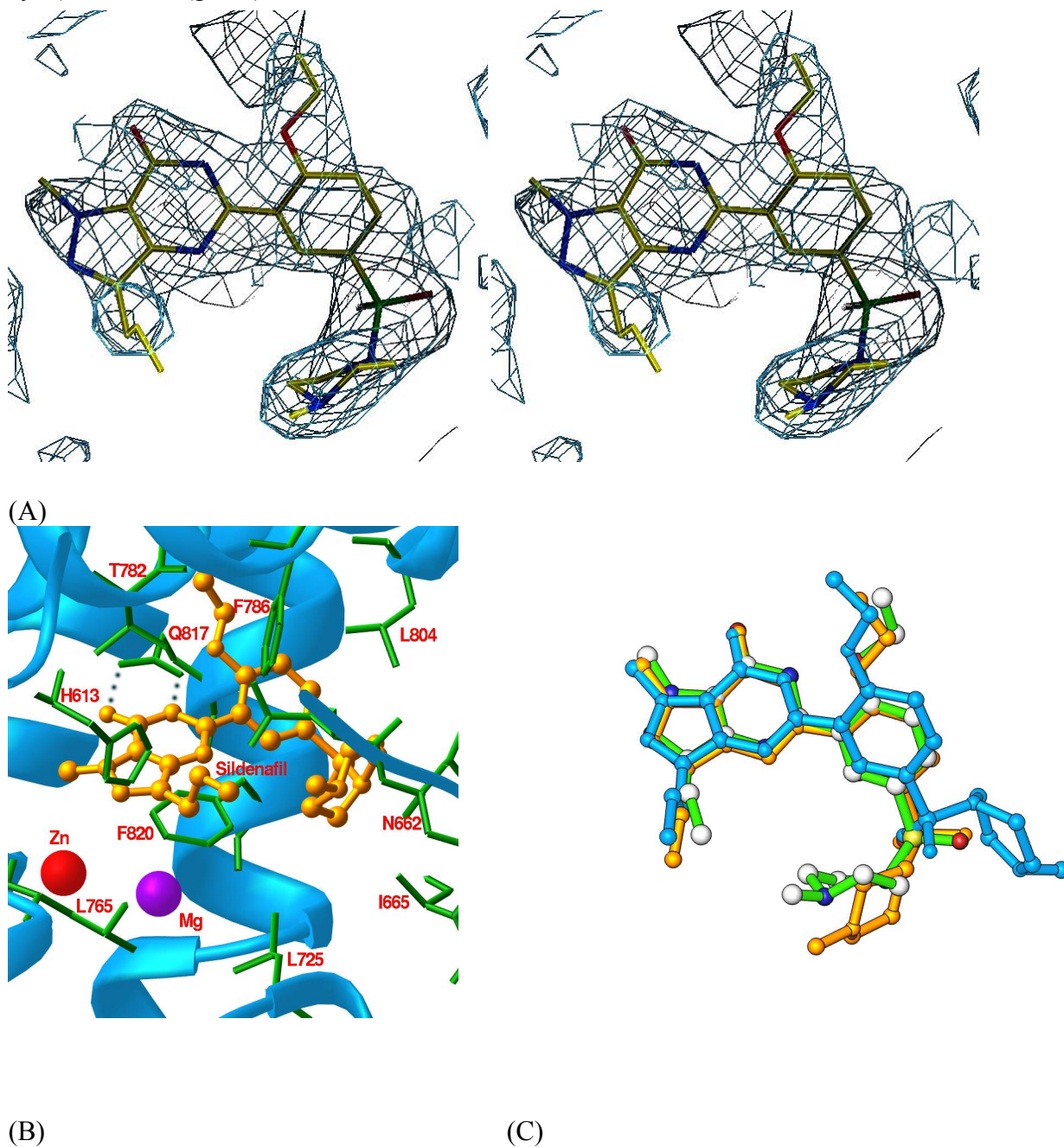
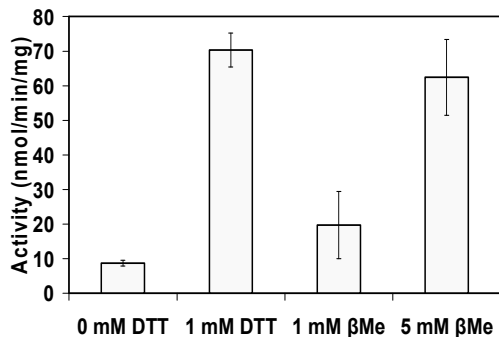
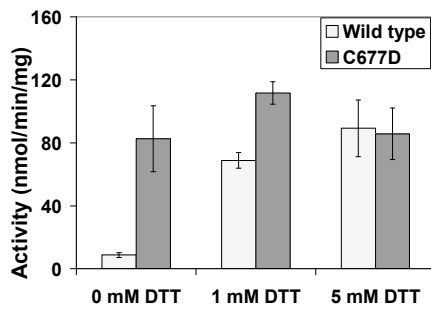


Figure 3.4. Effects of reducing agent on the activity of PDE5A. (A) The activity of PDE5A was increased 5-10 folds in the presence of reducing agents such as dithiothreitol and β -mercaptoethanol. (B) Mutation of Cys677 to aspartic acid (corresponding residue in PDE4) caused the loss of this effect. Specific activity was measured under the substrate concentration of 0.2 μ M cGMP.

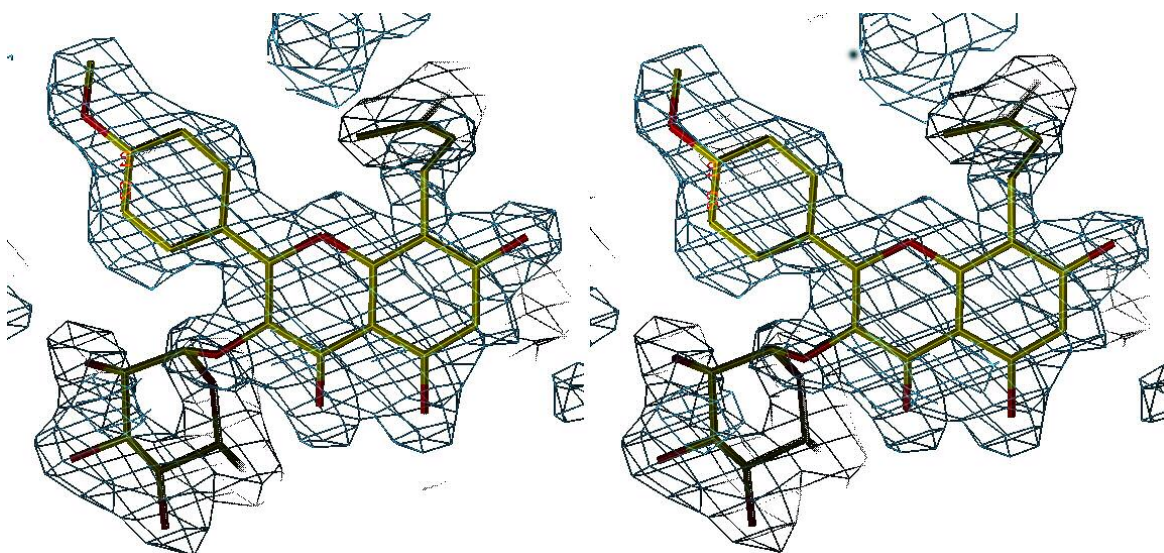


(A)

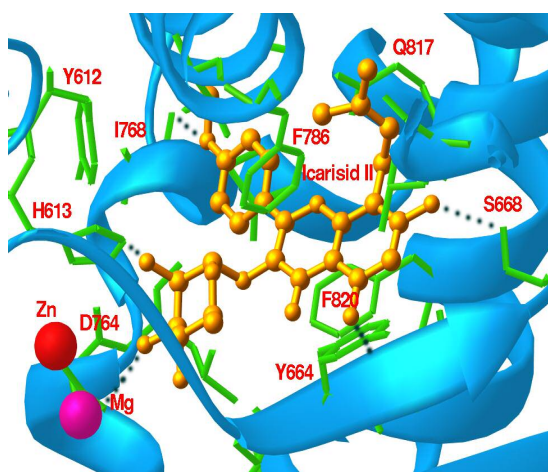


(B)

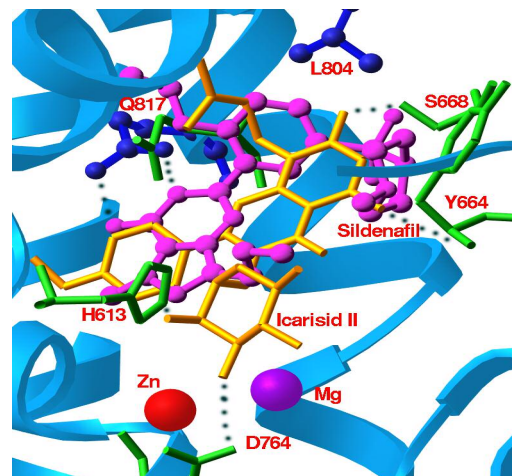
Figure 3.5. Icarisid II binding. (A) Stereoview of electron density for icarisid II bound to PDE5A1. The (2Fo-Fc) maps were calculated from the structure before icarisid II was built in and contoured at 1.5 σ . (B) Interaction of icarisid II (golden sticks-balls) with the PDE5A1 residues (green sticks) at the active site of PDE5A1. The dotted lines represent hydrogen bonds. (C) Superposition of icarisid II (golden sticks) and sildenafil (purple ball-sticks). Residues from PDE5A-sildenafil are shown in blue and residues from the icarisid II complex is drawn in green.



(A)



(B)



(C)

Figure 3.6. Inhibition of the isolated PDE5 catalytic domain of wild type and H-loop deletion mutants by IBMX, icaridisid II, and sildenafil.

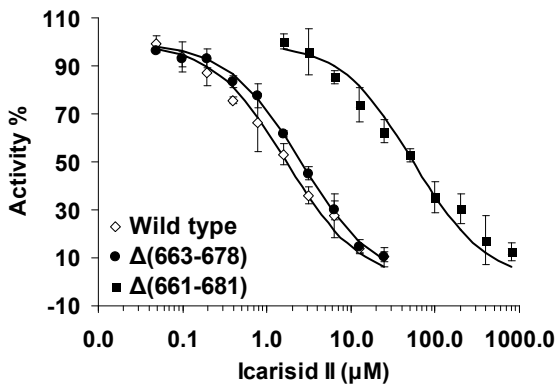
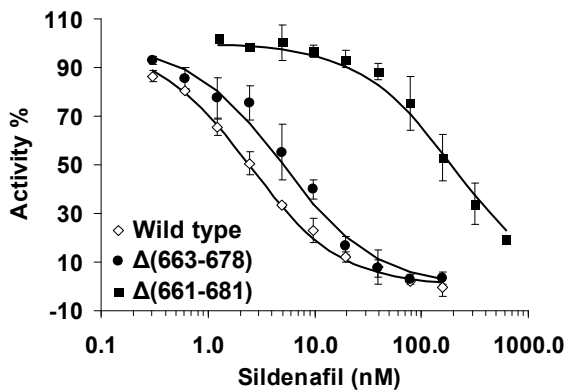
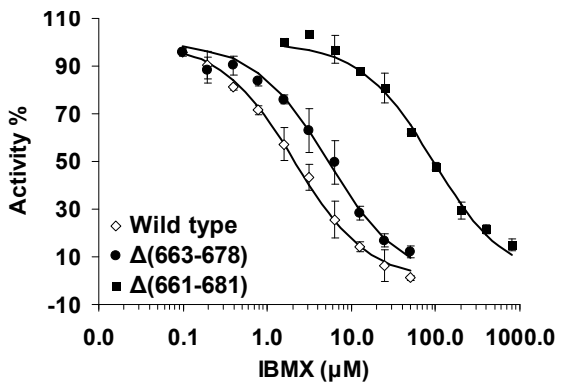


Table 3.1. Statistics on diffraction data and structure refinement.

Data collection	PDE5A1 native	PDE5A1-sildenafil	
PDE5A1-Icarisid II			
Space group	P3 ₁ 21	P6 ₂ 22	P6 ₁ 22
Unit cell (a, b, c, Å)	74.7, 74.7, 130.7	164.6, 164.6, 193.1	110.7, 110.7, 106.2
Resolution (Å)	1.85	2.3	1.8
Total measurements	363,960	1,121,219	412,999
Unique reflections	36,603	68,786	36,177
Completeness (%)	99.5 (100.0)*	99.9 (100.0)	99.9 (99.7)
Average I/σ	20.8 (7.4)*	6.7 (4.8)	13.6 (4.3)
Rmerge	0.058 (0.49)*	0.117 (0.58)	0.061 (0.46)
Structure Refinement			
R-factor	0.221	0.210	0.206
R-free	0.236 (9.7%)‡	0.246 (9.7%)	0.233 (9.7%)
Resolution (Å)	15-1.85	48-2.3	44-1.8
Reflections	34,996	66,315	35,094
RMS deviation for			
Bond	0.0078 Å	0.0061	0.0073
Angle	1.25°	1.17°	1.31°
Average B-factor (Å ²)			
Protein	37.5 (2523)§	27.8 (7804)	27.9 (2650)
Inhibitor		29.4 (99)	25.9 (37)
Waters	37.9 (148) §	28.8 (311)	32.8 (231)
Zn	46.2 (1)§	44.9 (3)	36.6 (1)
Mg	33.4 (1)§	37.6 (3)	41.0 (1)

*The numbers in parentheses are for the highest resolution shell.

‡The percentage of reflections omitted for calculation of R-free.

§The number of atoms in the crystallographic asymmetric unit.

Table 3.2. Interactions of sildenafil and icarisisid II with PDE5A.

Inhibitor	atoms	PDE5 atoms	Distance (Å)
Sildenafil	N4	Gln817 OE1	2.9
	O2	Gln817 OE1	3.2
	O1	Gln817 NE2	3.2
	O1	H ₂ O	2.7
	N1	H ₂ O	2.6
Icarisisid II	O1	Ile768 N	3.1
	O4	Ile665 N	2.8
	O10	Ser668 OG	3.0
	O7	His613 NE2	2.7
	O8	Asp764 OD2	2.8
	O8	H ₂ O	2.6
	O10	H ₂ O	2.7
Van der Waals' contacts:			
For sildenafil			
Pyrazolopyrimidinone	Tyr612, Leu765, Ala767, Val782, Gln817, Phe820		
Ethoxyphenyl	Val782, Ala783, Phe786, Leu804, Ile813, Gln817, Phe820		
methylpiperazine	Asn662, Ser663, Tyr664, Ile665, Leu804, Phe820		
For icarisisid II			
Methoxyphenyl	Ala767, Ile768, Gln775, Ala779, Val782, Gln817, Phe820		
Oxychromone	Tyr664, Ile665, Ser668, Leu725, Leu804, Met816, Phe820		
Pentenyl	Val782, Phe786, Leu804, Met816, Gln817		
Rhamnose	Tyr612, His613, Asn661, Ser663, Leu725, Asp764, Leu765, Phe786, Phe820		

Table 3.3. Kinetic properties of PDE5A1 isolated catalytic domain and its mutants.

	K_M^{cGMP} (μM)	k_{cat}^{cGMP} (sec^{-1})	$(k_{cat}/K_M)^{cGMP}$ ($\text{s}^{-1}\mu\text{M}^{-1}$)	IBMX ($\text{IC}_{50}\mu\text{M}$)	Icarisid II ($\text{IC}_{50}\mu\text{M}$)	Sildenafil (IC_{50}nM)
Wild type	5.1±1.3	1.3±0.3	0.27±0.08	2.1±0.5	1.7±0.4	2.4±0.3
$\Delta(663-678)^*$	54±6	3.8±0.5	0.07±0.013	5.3±1.1	2.5±0.2	5.9±1.5
$\Delta(661-681)^*$	750±210	2.3±0.6	0.0031±0.0002	95±6	55±13	188±29

*Four glycines were inserted as a linker. Each of the experiments was repeated three times.

CHAPTER IV

CRYSTAL STRUCTURES OF PDE10 IN COMPLEX WITH SUBSTRATES AND PDE4 SUBFAMILIES IN COMPLEX WITH A PDE4D-SELECTIVE INHIBITOR

4.1. Introduction

Structural studies on PDEs have been challenging because of difficulty in preparation of soluble PDE proteins. Most research groups expressed PDE proteins in insect cells. However, due to the low expression level of baculovirus systems, a large scale of purification for crystallographic study is a disadvantage for academic groups. Several groups purified PDEs by refolding or expressed PDEs using in vitro translation system (1,2). I have focused on expression of PDEs in *E. coli* and succeeded in purification of the catalytic domains of PDE2A3, PDE3A, PDE4 subfamilies A to D, PDE5A1, PDE7A1, PDE9A2, and PDE10A2. This chapter describes the recent progress on the crystal structures of PDE10A catalytic domain and its complex with cAMP and cGMP, and crystallization trials on the PDE4 subfamily members in complex with a PDE4D selective inhibitor.

4.2. Crystal structure of PDE10

Phosphodiesterase family 10 (PDE10) is mostly expressed in testis and brain (3-5). PDE10 contains two GAF domains preceded its catalytic domain. PDE10A hydrolyzes cGMP with a K_M of 3-7.2 μM and cAMP with a K_M of 0.05-0.26 μM (3-5), thus exhibiting dual-substrate selectivity. Up to date, neither crystal structures nor selective inhibitors of PDE10 have been reported. Therefore, substrate specificity and inhibitor selectivity of the PDE10 family remain unknown. Here, I report the crystal structure of the catalytic domain of PDE10A2 and the preparation of inactive D764A mutant of PDE10A catalytic domain. Crystals of the inactive PDE10A mutant in complex with both substrates of cAMP and cGMP are in progress. Since no structures of PDE families in complex with substrates or their analogs have been reported, these structures will not only provide insight into substrate specificity, but may also serve as templates for development of selective inhibitors of PDE10.

Expression, purification and crystallization of PDE10A2--The cDNA clone of human PDE10A2 (AB026816) was purchased from ATCC (IMAGE: 6106131). The catalytic domain of PDE10A2 (residues 448-789) was subcloned into vector pET15b. The *E. coli* cell carrying pET-PDE10A2 was grown in 2xYT medium at 37°C to absorption $A_{600} = 0.7$ and then 0.1 mM isopropyl β -D-thiogalactopyranoside was added for further growth at 20°C overnight. The *E. coli* cell was resuspended in ice-cold lysis buffer (20 mM Tris.HCl, pH 8.0, 15 mM imidazole, 50 mM NaCl, 1 mM β -mercaptoethanol, plus protease inhibitor mixture), centrifuged after lysed by French Press. The supernatant was loaded into a Ni-NTA agarose (Qiagen) column and eluted with 150 mM imidazole. Eluted PDE10A2 protein was digested

by thrombin to cleave out the 6×His tag. The resulted PDE10A2 was loaded into Q-Sepharose ion exchange column and eluted with 20 mM Tris.HCl, pH 7.5, 1 mM β-mercaptoethanol , 1 mM EDTA and 100 mM NaCl. The partial purified PDE10A2 proteins was concentrated and further loaded into Sephacryl S300 (Amersham Biosciences) size exclusive column (95cM × Φ2.5cM) and eluted with a buffer of 20 mM Tris.HCl, pH 7.5, 1 mM β-mercaptoethanol , 1 mM EDTA and 50 mM NaCl. The catalytic domain of PDE10A2(448-789) was eluted at the fraction numbers 53-59 (6.5 mL/fractions), which was comparable with molecular weight of a monomer(~39Kd). The PDE10A2 protein had purity greater than 95% as shown by SDS-PAGE. A typical batch of purification yielded over 10 mg PDE10A2 from a 2-liter cell culture.

The mutant PDE10A2(448-789)D674A were produced by the standard protocol of site-directed mutagenesis (QuikChange site-directed mutagenesis kit (Stratagene)). Overexpression and purification of the mutant PDE10A2 were used the same protocols as for the wild type protein.

The catalytic domain of PDE10A2 and its mutant was crystallized by hanging drop at 4°C. The protein drops contained 2 μl of 7 mg/ml PDE10A2 and 2 μl well buffer of 0.1 M HEPES (pH 7.5), 0.1-0.2 M MgCl₂, 25-200 mM β-mercaptoethanol and 10-20% PEG 3350. The PDE10A2 crystal diffracts to 2.2 Å resolution in our RAXIS4⁺⁺ system with a cryosolvent 0.1 M HEPES (pH 7.5), 0.1 M MgCl₂, 25 mM β-mercaptoethanol, 20% PEG 3350 and 20% Ethylene Glycol. The crystal has the space group P2₁2₁2₁ with a =51.1, b =82.1, and c = 155.2 Å. The structure of PDE10 was determined by molecular replacement

program AmoRe (6), using the catalytic domain of PDE5A as the searching model. The structure was refined by program CNS (7) to R-factor/R-free of 0.22/0.27 at 2.2 Å resolution (Table 4.1). The crystal of the mutant PDE10A2(448-789)D674A has a space group $P2_12_12_1$ with $a = 51.4$, $b = 82.1$, and $c = 155.3$ Å. For PDE10A/cAMP or PDE10A/cGMP complexes, the crystal of the mutant was soaked with 20-50 mM cAMP or cGMP at 4°C or 25°C for 1-8 hours with a soaking buffer 15% PEG8000, 0.06 M HEPES (pH 7.5), 0.06 M $MgCl_2$, 30 mM β -mercaptoethanol, 30 mM NaCl, 12 mM Tris-HCl (pH 7.5), 0.6 mM EDTA. The cryosolvent is similar with the soaking buffer in addition to 20% PEG400.

Results and discussion--The crystal of the PDE10A2 catalytic domain contains two protein molecules per asymmetric unit. The crystal packing shows that the catalytic domain of PDE10A2 is a dimer (Figure 4.1). The catalytic domain of PDE10A2 is composed of fifteen α -helices and five 3_{10} helices. The overall folding of the catalytic domain of PDE10, except for the N-terminus, is similar to those of other seven PDE families whose structures are known. The variation of the N-termini in the catalytic domains of PDEs possibly reflects structural differences across PDE families. In PDE10, the corresponding residues of the H-loop in PDE5 adopt two α -helices, which is similar to PDE4, consistent with that the H-loop in PDE5 is unique across all known structures of the catalytic domain of PDEs (Figure 1.6). Further structure analysis is in progress.

Because PDEs present a k_{cat} value around 1 sec^{-1} , the time scale of crystallization as well as soaking will be enough for PDEs to hydrolyze the substrate completely. Therefore, only PDEs in complex with a product have been reported (8, 9). To achieve a complex structure of

a PDE with the substrate cAMP or cGMP, I mutated a residue D674A in PDE10A2, which is responsible for binding of a metal ion and for hydrolysis of substrates, but expected to play little role in substrate binding (8, 9). The mutant PDE10A2 has a specific activity $3.2 \pm 0.5 \times 10^{-5}$ $\mu\text{mol}/\text{min}/\text{mg}$ for cAMP, which is about 1.5×10^4 less than wild type (0.48 ± 0.01 $\mu\text{mol}/\text{min}/\text{mg}$). The crystal of the mutant PDE10A2 was soaked with cAMP and cGMP and the ligand binding has been observed. We are planning to collect higher quality data on a synchrotron source.

4.3. Studies on subfamily selectivity of PDE4 inhibitors

PDE4 inhibitors have shown great potential for treatment of asthma and chronic obstructive pulmonary disease (10-16), but side effects such as emesis are the main obstacles for PDE4 inhibitors to be drugs used in practical treatment. While mechanisms for the side effects are not clear, selective inhibition on one of four subfamilies of PDE4 has become the current focus of PDE4 inhibitor development (11-13, 17). However, only a few subtype selective PDE4 inhibitors have been reported (18) and no structures of PDE4 in complex with subfamily selective inhibitors are available, thus leaving subfamily selectivity as a veiled puzzle. Absolute conservation of the rolipram binding residues in the PDE4 subfamilies suggests that the subfamily selectivity is largely dependent on the conformational states of the PDE4 subfamilies. To elucidate the basis of PDE4 subfamily selectivity and to provide templates for design of PDE4 subfamily specific inhibitors, I target to determine the structures of PDE4 subfamilies (A, B, C, and D) in complex with a PDE4 subfamily selective inhibitor. Herein, I describe the preliminary processes on expression of the catalytic domains of PDE4 subfamilies A to D and crystallization of PDE4A-D in complex with a PDE4D subfamily inhibitor.

Expression and purification of PDE4A, PDE4B, PDE4C and PDE4D--There exist the protocols for overexpression of the catalytic domain of PDE4B and PDE4D2 in Dr. Ke's lab. I reconstructed PDE4B and PDE4D2 to obtained crystals that diffract to higher resolution. The cDNA clone of human PDE4A10 (BF528806) was purchased from ATCC. The cDNA clone of human PDE4C2 was provided by Dr. Miles Houslay at University of Glasgow, UK. The catalytic domains of PDE4A10 (residues 290-622), PDE4B (residues 152-487), PDE4C2

(residues 200-558), and PDE4D2 (residues 86-413) were cloned into the expression vector pET15b, following the standard methods. The plasmids of pET-PDE4A10, pET-PDE4B2B, pET-PDE4C2, and PDE4D2 were transferred into *E. coli* strain BL21 (Codonplus) and expressed in LB medium at 11°C-15°C for 20-38 hours. The recombinant PDE4A10, PDE4B2B, PDE4C2, and PDE4D2 were purified by the columns of Ni-NTA agarose, Q-sepharose, and Sephacryl S300. A typical batch of purification from a 2 liter cell culture yielded 10 mg PDE4A10, 20 mg PDE4B, 15 mg PDE4C2, and 50 mg PDE4D. The purified proteins have a purity of >95%.

Crystallization of PDE4A-4D in complex with PDE4D subfamily selective inhibitors

--Novartis' inhibitor NVP-ABE171 (4-(8-benzo[1,2,5]oxadiazol-5-yl-[1,7]naphthyridine-6-yl)-benzoic acid, Figure 4) is the best PDE4 subfamily-selective inhibitor and has IC₅₀ values of 602, 34, 1230, and 1.5 nM for PDE4A, 4B, 4C, and 4D (23). Crystals of the catalytic domains of PDE4A, PDE4B, PDE4C, and PDE4D in complex with NVP-ABE171 have been grown by hanging drop. The complexes were prepared by mixing 70 mg/ml PDE4A10 (290-622), 10 mg/ml PDE4B2B (152-487), 15 mg/ml PDE4C2 (200-538), or 12 mg/ml PDE4D2 with 2-3.5 mM NVP-ABE171. The following well buffers were used for crystallization: 12% PEG400, 200 mM Mg acetate, 0.1 HEPES pH 7.5, 5% glycerol for PDE4A10; 10-15% PEG3350, 0.1 HEPES pH 7.5, 30% ethylene glycol, 20% isopropanol at 4°C for PDE4B2B, 10-15% PEG3350, 100 mM MgCl₂, 0.1 HEPES pH 7.5 at room temperature for PDE4C2; and 18-22% PEG3350, 0.1 HEPES pH 7.5, 30% ethylene glycol, 10% isopropanol, 200 mM MgCl₂ at 4°C for PDE4D2. The PDE4A10 crystals have the space group P4₁2₁2 with a = b = 105 and c = 164 Å and diffracted to 2.6 Å resolution in our Raxis

IV⁺⁺ system. The PDE4B2B crystals have a space group P4₃2₁2 with a=b=54 and c=237 Å and diffracted up to 2.0 Å. The PDE4C2 crystals have a hexagonal system with a = b = 74 and c = 272 Å and diffracted to 3.2 Å resolution in our Raxis IV⁺⁺ system. The PDE4D2 crystals have the space group of P2₁2₁2₁ with a = 59, b = 82, c = 162 Å, and diffracted to 2.0 Å resolution in our Raxis IV⁺⁺ system. Improvement of crystallization conditions are in progress. We plan to collect higher resolution data of PDE4A, 4B, 4C and 4D in complex with NVP-ABE171 on a synchrotron beam line.

REFERENCES

1. Iffland A, Kohls D, Low S, Luan J, Zhang Y, Kothe M, Cao Q, Kamath AV, Ding YH, Ellenberger T. (2005) *Biochemistry* 44, 8312-8325.
2. Scapin G, Patel SB, Chung C, Varnerin JP, Edmondson SD, Mastracchio A, Parmee ER, Singh SB, Becker JW, Van der Ploeg LH, Tota MR. (2004) *Biochemistry* 43, 6091-6100.
3. Loughney, K., Snyder, P. B., Uher, L., Rosman, G. J., Ferguson, K., & Florio, V.A. (1999) *Gene*. 234:109-17.
4. Soderling, S.H. , Bayuga S. J. & Beavo J.A. (1999) *Proc. Natl. Acad. Sci.* 96:7071-6.
5. Fujishige K., Kotera J., Michibata H., Yuasa K., Takebayashi S., Okumura K. & Omori K. (1999) *J. Biol. Chem.* 274:18438-45.
6. Navaza, J. & Saludjian, P. (1997) *Methods Enzymol.*, 276, 581-594.
7. Brünger, A.T., Adams, P.D., Clore, G.M., DeLano, W.L., Gros, P., Grosse-Kunstleve, R.W., Jiang, J.S., Kuszewski, J., Nilges, M., Pannu, N.S., Read, R.J., Rice, L.M., Simonson, T., and Warren, G.L. (1998) *Acta Cryst.* D54, 905-921.
8. Huai, Q., Colicelli, J., and Ke, H. *Biochemistry* 42, 13220-13226 (2003).
9. Zhang, K.Y., Card, G.L., Suzuki, Y., Artis, D.R., Fong, D., Gillette, S., Hsieh, D., Neiman, J., West, B.L., Zhang, C., Milburn, M.V., Kim, S.H., Schlessinger, J., and Bollag, G. (2004) *Mol. Cell* 15, 279-286.
10. Barnette, MS. (1999) *Fortschritte der Arzneimittelforschung - Progress in Drug Research*, 53, 193-229,
11. Barnette, M. S., Underwood, D. C. (2000) *Curr. Opin. Pulmonary Med.*, 6, 164-169.
12. Huang, Z., Ducharme, Y., MacDonald, D., and Robinchaud, A. (2001) *Curr. Opin. Chem. Biol.*, 5, 432-438.
13. Giembycz, M. A. (2002) *Monaldi Arch. Chest Dis.* 57, 48-64.
14. Piaz, V. D. & Giovannoni, P. (2000) *Eur. J. Med. Chem.*, 35, 463-480.
15. Souness, J. E., Aldous, D., & Sargent C. (2000) *Immunopharmacology*, 47, 127-162.
16. Sturton, G. & Fitzgerald, M. (2002) *Chest*, 121, 192s-196s.
17. Lipworth B.J. (2005) *Lancet*. 365:167-75.

18. Trifilieff, A., Wyss, D., Walker, C., Mazzoni, L. & Hersperger, R. (2002) *J. Pharmacol. Exp. Ther.* 301:241-8.

Figure 4.1. Ribbon diagram of the catalytic domain of PDE10A. The crystal packing shows that the catalytic domain of PDE10A2 is dimeric. Zn is colored blue and Mg is yellow.

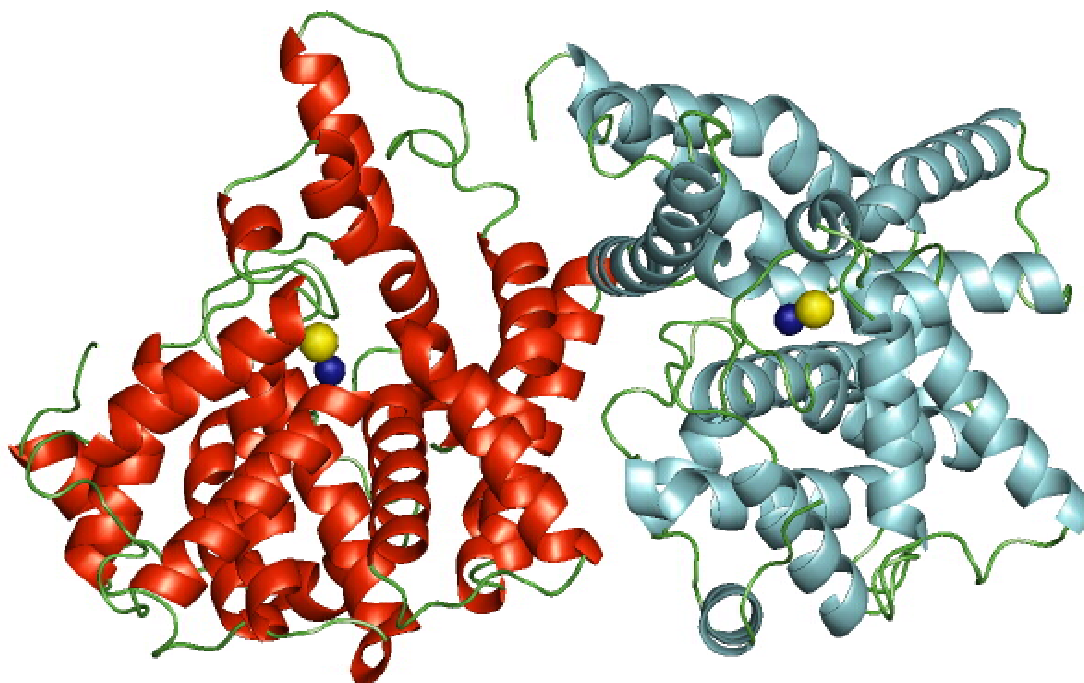


Figure 4.2. Chemical structure of a PDE4D-selective inhibitor NVP-ABE171. The IC_{50} values are 602 nM, 34 nM, 1230 nM and 1.5 nM for PDE4A, B, C and D, respectively.

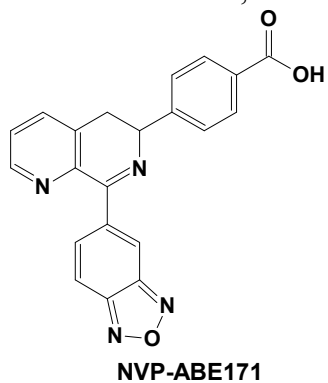


Table 4.1. Statistics on diffraction data and structure refinement of PDE10A2(448-789).

Space group	P2 ₁ 2 ₁ 2 ₁
Unit cell (a, b, c, Å)	51.1, 82.1, 155.2
Resolution (Å)	2.2
Total measurements	130,805
Unique reflections	31,826
Completeness (%)	89.3 (62.3)
Average I/σ	4.2(2.6)*
Rmerge	0.108(0.469)*
Structure Refinement	
R-factor	0.215
R-free	0.271 (9.0%)‡
Resolution (Å)	99-2.2
Reflections	30,263
RMS deviation for	
Bond	0.0063Å
Angle	1.21°
Average B-factor (Å ²)	
Protein	27.5(5244)§
Waters	24.7(192) §
Zn	29.6 (2)§
Mg	22.6 (2)§

*The numbers in parentheses are for the highest resolution shell.

‡The percentage of reflections omitted for calculation of R-free.

§The number of atoms in the crystallographic asymmetric unit.

CHAPTER V
OTHER WORKS I CONTRIBUTED TO

Listed as follows are my contributions to other work that has been published.

1. **The PDE4D2 structure in complex with enantiomer inhibitors.** Huai Q, Sun Y, Wang H, Macdonald D, Aspiotis R, Robinson H, Huang Z, Ke H. Enantiomer Discrimination Illustrated by the High Resolution Crystal Structures of Type 4 Phosphodiesterase. *J Med Chem.* 49(6):1867-1873.

2. **The structure of E coli hsp90.** Huai, Q., Wang, H., Liu, Y., Kim, H. Y., Toft, D., and Ke, H. (2005) Structures of the N-terminal and middle domains of E. coli Hsp90 and conformation changes upon ADP binding. *Structure* **13**, 579-590.

3. **The PDE9 structure.** Huai, Q., Wang, H., Zhang, W., Colman, R., Robinson, H., and Ke, H. (2004) Crystal structure of phosphodiesterase 9 shows orientation variation of inhibitor 3-isobutyl-1-methylxanthine binding. *Proc. Natl. Acad. Sci. USA*, **101**, 9624-9629.

4. **The DJ-1 structure.** Huai, Q., Sun, Y., Wang, H., Chin, L. S., Li, L., Robinson, H., and Ke, H. (2003) Crystal structure of DJ-1/RS and implication on familial Parkinson's disease. *FEBS Lett.* **549**, 171-175.

5. **The PDE4D2 structure in complex with inhibitor rolipram.** Huai, Q., Wang H., Sun, Y., Kim, H.Y., Liu, Y., and Ke, H. (2003) Three dimensional structures of PDE4D in complex with roliprams and implication on inhibitor selectivity. *Structure* **11**, 865-873.

6. **The crystal structure of a complex involving a mouse TCR and a human MHC molecule.** Buslepp, J., Wang, H., Biddison WE, Appella, E. and Collins, E.J. (2003) A correlation between TCR Valpha docking on MHC and CD8 dependence: implications for T cell selection. *Immunity* **19**:595-606.